Isotropic distributions for 3-dimension rotations and one-sample Bayes inference

by

Yu Qiu

A dissertation submitted to the graduate faculty

in partial fulfillment of the requirements for the degree of

DOCTOR OF PHILOSOPHY

Major: Statistics

Program of Study Committee:
Stephen B. Vardeman, Co-major Professor
Daniel J. Normdan, Co-major Professor
Peng Liu
Max Morris
Huaiqing Wu

Iowa State University

Ames, Iowa

2013

DEDICATION

I would like to dedicate this thesis to my husband Yun and to my daughter Grace without whose support I would not have been able to complete this work. I would also like to thank my family and friends for their loving guidance and financial assistance during the writing of this work.

TABLE OF CONTENTS

ABSTRACT

This dissertation discusses models for 3-dimensional orientations. A new Uniform-Axis-Random-Spin (UARS) family is developed and the corresponding Bayes inferences for all UARS distributions are studied. The effectiveness of one-sample non-informative Bayes methods are demonstrated which indicates the broad use in material science. Finally an `R` package has been developed which is useful for practical modelers.

CHAPTER 1. INTRODUCTION

Organization

This dissertation is organized as a collection of journal-submission-ready papers. The first paper,"A Wrapped Trivariate Normal Distribution for 3-D Rotations and Bayes Inference" introduces a new family of isotropic distributions within the UARS class and compares it to other isotropic distributions in the literature. Also the one-sample Bayes inference for the new family has been studied. The second paper, "One-Sample Bayes Inference for Symmetric Distributions of 3-D Rotations" illustrates the use of one-sample Bayes method for all the isotropic distributions on 3-D rotations. The third paper, "Uarsbayes: A `R` Package for 3-D Orientation Data" provides a `R` package for practitioner to use.

CHAPTER 2. A WRAPPED TRIVARIATE NORMAL DISTRIBUTION FOR 3-D ROTATIONS AND BAYES INFERENCE

A paper submitted to *Statistic Sinica*

Yu Qiu, Daniel J. Nordman and Stephen B. Vardeman

Abstract

For modeling orientation data (data points represented as 3×3 rotation matrices), we develop a wrapped trivariate normal distribution (wTND) for rotationally symmetric "errors" in random rotations, having a simple geometric construction. While of interest in its own right, the wTND also provides simple and effective approximations of the isotropic Gaussian distribution on rotations, with some advantages over approximations based on other commonly used models for rotations. (While some literature has suggested the contrary, we explain that the isotropic Gaussian distribution has a central limit theorem-based motivation for modeling rotations, though its distributional form is complicated.) We develop non-informative Bayes inference for the wTND via Markov Chain Monte Carlo methods, which allow straightforward computations in a model where maximum likelihood is undefined. Credible regions for model parameters (including a fixed 3×3 central or "mean" rotation) are shown to possess good frequentist coverage properties. As an interesting feature, the wTND can exhibit both regular and non-regular behavior, depending upon the degree of variation in the underlying rotations, and empirical convergence rates vary from regular $n^{-1/2}$ rates to non-regular super-efficient n^{-1} rates. We illustrate the model and inference method with real orientation data collected in texture analysis from materials science.

1 Introduction

Three-dimensional orientation data are of interest in a wide variety of fields including human kinematics, vectorcardiography, structural geology, robotics and materials science (cf. Downs, 1972; Chang, 1998; Matthies et al., 1988; Rancourt et al., 2000; Stavdahl et al., 2005; Bingham et al., 2009a); see Mardia & Jupp (2000, Sec. 13.2.1) for an introduction. With such data, each observation is represented by a 3×3 rotation matrix in $SO(3)$ (i.e., the set of an orthogonal matrices with determinant 1) and typically denotes the orientation of some object after rotating its reference frame in $\mathbb{R}^3$ away from some "world" reference frame. For clarity in what follows, we will refer to a probability model for a random 3×3 rotation matrix as a *rotational distribution*.

In the statistical literature, the oldest and most well-studied parametric family of rotational distributions is the Matrix Fisher family, introduced by Downs (1972) and examined by Khatri & Mardia (1977) and Jupp & Mardia (1979). In many applications involving orientation data, rotational distributions used are symmetric or *isotropic* (i.e., having central or rotationally invariant densities) about a central rotation in $SO(3)$, and intended to model the variability in orientation data as due to directionally symmetric random pertubations of an underlying mean rotation parameter. Using such rotational distributions is akin to using errors ε, symmetrically distributed around 0 in a standard location model $Y = \mu + \varepsilon$ for real-valued data. In the statistical literature, the common distributions on $SO(3)$ of this form are the isotropic versions of the Matrix Fisher (arguably the most popular) and Cayley distributions (cf. Downs, 1972; León et al. 2006, sec. 5.2), though other such models include Bunge's Gaussian distribution (Bunge, 1982), the Lorentzian distribution (Matthies, 1982), the de la Vallée Poussin distribution (Schaeben, 1997) and the isotropic Gaussian (or circular normal) distribution on $SO(3)$ (related to the even Brownian motion distribution on S^3, the $\mathbb{R}^4$-unit sphere) (cf. Savyolova, 1984; Matthies et al., 1988; Schaeben, 1992; Nikolayev & Savyolova, 1997; Borovkov & Savyolova, 2007). All of these belong to a general class of isotropic distributions on $SO(3)$, referred to here as "uniform-angle-random-spin" (UARS) distributions, which have intuitive interpretation as random "rotational errors" as well as a simple geometric construction in terms of

Euler's axis-angle representation of rotations; see, for example, León et al. (2006, sec. 5.2), Bingham et al. (2009a) and Hielscher et al. (2010). Such rotational distributions are also equivalent to rotationally symmetric distributions on quaternions (or S^3) and their mapping to $SO(3)$ (cf. Section 2.1; Mardia, 1975; Watson, 1983; Prentice, 1986; Schaeben, 1992; Schaeben & Nikolayev, 1998, sec. 6.2).

Our purposes in this manuscript are two-fold. First, we wish to clarify the isotropic Gaussian distribution (IGD) on $SO(3)$, which is a rotational distribution from texture analysis that is not widely appreciated in the statistical literature. An appealing property of this distribution for modeling orientations is its position as a type of "normal" distribution for rotations, by serving as the distributional limit for compositions of large numbers of independent, small random rotations. However, since its proposal (Savyolova, 1984; Matthies et al., 1988; Nikolayev & Savyolova, 1997), the IGD on $SO(3)$ has been criticized as having no motivation through a meaningful central limit theorem (CLT) argument with rotations (cf. Shaeben, 1992; Schaeben & Nikolayev, 1998). We point out that there is indeed a simple, rigorous argument showing that the IGD on $SO(3)$ can *legitimately* be motivated as the limit distribution obtained by a CLT using UARS-orientations to provide natural types of small, independent random rotations for compositions. Hence, the IGD on $SO(3)$ does have a real CLT-related motivation for modeling orientation data, giving it the same kind of justification as is usually provided for the normal and log-normal distributions in other statistical modeling applications.

Our second and main aim in this paper is to develop a new family of isotropic distributions on $SO(3)$ (i.e., a family within the UARS class), referred to here as the wrapped trivariate normal distribution (wTND) class. These rotational distributions are motivated by a CLT in $\mathbb{R}^3$, rather than a CLT in $SO(3)$ directly, along with an exponential mapping (and wrapping) of $\mathbb{R}^3$ onto $SO(3)$. One major motivation for the wTND is that it has a fairly simple distributional form for statistical inference, unlike the IGD on $SO(3)$ that has a rather complicated density (as is noted in Matthies et al. (1988) and Borovkov & Savyolova (2007)). The wTND also turns out to closely approximate the IGD on $SO(3)$ in many practical situations, more so than many other commonly used isotropic models for rotations. We view such approximations

of the IGD on $SO(3)$ as useful, not only because IGD on $SO(3)$ has CLT motivations, but also (and relatedly) because *any* highly concentrated UARS distribution for rotational errors with a continuously differentiable density will closely follow the IGD on $SO(3)$ (see Section 2.2). Many of the UARS models mentioned above (e.g., Bunge's Gaussian, Lorentzian and even the IGD) fail to have simple parametric densities for statistical inference (cf. Section 2.1, 3.2), and so the wTND model can become a tractable substitute for highly concentrated orientations. Implicit assumptions involving trivariate normal distributions have also appeared for approximating highly concentrated Matrix Fisher distributions and subsequently deriving approximate confidence regions and tests (Rancourt et al., 2000); see also Chang & Rivest (2001, sec. 4). On $SO(3)$, this is an analog of modeling concentrated spherical data with wrapped normal distributions (Jupp & Mardia, 1989). However, by directly considering the wTND for rotational data, a parametric model emerges in its own right along with exact parametric inference for this model. These have not been considered in the existing literature.

We then describe one-sample Bayes inference for the wTND, using non-informative priors on the two parameters of the distribution. One (the location) parameter is a fixed mean rotation $\mathbf{S} \in SO(3)$ and the other parameter $\kappa \in (0, \infty)$ controls the concentration (variability) of random rotations from the wTND. Because the parameter $\mathbf{S}$ lies in $SO(3)$, we use Bayes inference for the pragmatic reasons that 1) the approach is straightforward to implement computationally, 2) no decompositions or parameterizations of $\mathbf{S} \in SO(3)$ are required (e.g., Euler angles, Cayley transforms, exponential maps or quaternions) as is otherwise typical of likelihood approaches, and 3) the method allows one to directly construct credible regions for $\mathbf{S} \in SO(3)$ which have simple geometric interpretations. Simulations also indicate that, with the non-informative priors, the resulting Bayes credible regions have excellent frequentist properties.

The rest of the manuscript is organized as follows. Section 2 describes the UARS-framework for isotropic distributions on $SO(3)$ and provides a CLT motivation for the IGD on $SO(3)$. Section 3 provides the wTND along with some simulation studies indicating the effectiveness of its approximation to the IGD on $SO(3)$ compared to some competing approximations.

In Section 4, we outline one-sample Bayes inference for the wTND, using non-informative priors. Interestingly, the credible regions for the mean rotation parameter $\mathbf{S} \in SO(3)$ can have average sizes which effectively exhibit both regular and unusually fast (i.e., non-regular) convergence rates, depending upon the concentration parameter $\kappa > 0$ involved. Section 5 examines the Bayes inference procedure and illustrates our findings through a substantial simulation study. Section 6 briefly illustrates the application of wTND for real orientation data collected in texture analysis, and Section 7 provides concluding remarks. An on-line Supplementary Appendix contains some additional results and proofs.

2 Preliminaries: UARS Models and IGD on $SO(3)$

2.1 The UARS Class: Rotationally Symmetric Models on $SO(3)$

"Uniform-angle-random-spin" (UARS) distributions for random rotations can be simply described using a stochastic version of Euler's angle-axis representation for rotations. For $\mathbf{v} = (v_1, v_2, v_3)^T \in \mathbb{R}^3$, define a mapping

$$\mathbf{A}(\mathbf{v}) = \begin{pmatrix} 0 & -v_3 & v_2 \\ -v_3 & 0 & -v_1 \\ -v_2 & v_1 & 0 \end{pmatrix}$$

of $\mathbb{R}^3$ to the space $so(3)$ of (real-valued) skew-symmetric 3×3 matrices, and define the matrix exponential

$$\exp(\mathbf{B}) = \sum_{k=0}^{\infty} \frac{1}{k!} \mathbf{B}^k$$

for $\mathbf{B} \in so(3)$. Then,

$$\exp(\mathbf{A}(\mathbf{v})) = (\cos \|\mathbf{v}\|)\mathbf{I}_3 + \frac{\sin \|\mathbf{v}\|}{\|\mathbf{v}\|}\mathbf{A}(\mathbf{v}) + \frac{1 - \cos \|\mathbf{v}\|}{\|\mathbf{v}\|^2}\mathbf{v}\mathbf{v}^T$$

represents a rotation of the identity matrix $\mathbf{I}_3$ (i.e., the set of standard coordinate vectors in $\mathbb{R}^3$) by an angle of $\|\mathbf{v}\|$ about a vector (or signed axis) $\mathbf{v} \in \mathbb{R}^3$ (following right-hand rule,

cf. Mardia & Jupp, 2000, p. 287). Then, letting $\mathbf{u} = (u_1, u_2, u_3)^T$ be uniformly distributed over the $\mathbb{R}^3$-unit sphere S^2 and, independently, letting r denote a random draw from an *angular distribution* on $(-\pi, \pi]$ having a symmetric density $g(\cdot|\kappa)$ whose spread is controlled by the concentration parameter $\kappa > 0$, a random UARS rotation with mean direction $\mathbf{I}_3$ is given by

$$\mathbf{M}(r, \mathbf{u}) \equiv \exp(\mathbf{A}(r\mathbf{u})) = (\cos r)\mathbf{I}_3 + (\sin r)\mathbf{A}(\mathbf{u}) + (1 - \cos r)\mathbf{u}\mathbf{u}^T, \tag{1}$$

a rotation by a random angle r about a random vector $\mathbf{u} \in \mathbb{R}^3$. This construction is subsequently used to define a UARS distribution with mean rotation $\mathbf{S} \in SO(3)$ (a fixed parameter) by $\mathbf{O} = \mathbf{S} \cdot \mathbf{M}(r, \mathbf{u})$ (or equivalently $\mathbf{M}(r, \mathbf{u}) \cdot \mathbf{S}$), representing a directionally symmetric perturbation of $\mathbf{S}$. We refer to the rotational distribution of $\mathbf{O}$ as a UARS model with parameters $\mathbf{S} \in SO(3)$, and angular density $g(\cdot|\kappa)$.

As an important feature of UARS models, each rotational distribution in the UARS class is completely characterized by some angular distribution in the definition (1), and all of the previously mentioned common families of isotropic distributions on $SO(3)$ (e.g., isotropic Matrix Fisher, Cayley, Bunge's Gaussian and IGD) correspond to different choices of angular densities $g(\cdot|\kappa)$ defined on $(-\pi, \pi]$ and symmetric around zero; these are listed in Table 1. Given an angular density $g(\cdot|\kappa)$ on $(-\pi, \pi]$ and mean rotation parameter $\mathbf{S} \in SO(3)$, a UARS rotation $\mathbf{O}$ has a corresponding density on $SO(3)$ given by

$$f(\mathbf{O}|\mathbf{S}, \kappa) = \frac{4\pi}{3 - tr(\mathbf{S}^T\mathbf{O})} g(\arccos[2^{-1}(tr(\mathbf{S}^T\mathbf{O}) - 1)]|\kappa), \quad \mathbf{O} \in SO(3) \tag{2}$$

with respect to the uniform distribution on $SO(3)$ which provides a dominating measure on $SO(3)$ (Downs, 1972); the uniform distribution is generated using $f(r) = [1 - \cos(r)]/[2\pi]$, $r \in (-\pi, \pi]$, in (1) and its density on $SO(3)$ is $f(\mathbf{O}) = 1$ from (1) with $\mathbf{S} = \mathbf{I}_3$ (Miles, 1965).

We thank referees for suggesting other generalizations and characterizations of UARS distributions. If a random variable t has a density $\tilde{g}(t)$ (with respect to the Lebesgue measure on $\mathbb{R}$) and, independently, $\mathbf{u}$ is uniformly distributed on S^2, then $\mathbf{S}\exp(\mathbf{A}(t\mathbf{u}))$ is UARS-distributed

Table 1 Angular density functions, with indicated concentration parameters, for the random angle $r \in (-\pi, \pi]$ defining common UARS models (1) on $SO(3)$. (Below I_i denotes the modified Bessel function of order i; $C(\cdot)$ denoted a normalizing constant; and $\lambda = \lambda(\kappa_L) = \kappa_L/2 - 0.5 + 2/(\kappa_L + 2)^2$ puts the Lorentzian distribution on roughly the same scale as the others, though the Lorentzian shape differs from the others for large concentrations κ_L.)

Model	Angular Density
[a]Isotropic Cayley (κ_C) or [b]de la Vallée Poussin	$\frac{1-\cos r}{2\pi} \frac{\sqrt{\pi}\Gamma(2\kappa_C^2+2)(1+\cos r)^{2\kappa_C^2}}{2^{2\kappa_C^2}\Gamma(2\kappa_C^2+1/2)}$
[c]Isotropic Matrix Fisher (κ_F)	$\frac{1-\cos r}{2\pi} \frac{\exp(\kappa_F^2 \cos r)}{I_0(\kappa_F^2) - I_1(\kappa_F^2)}$
[d]Bunge's Gaussian (κ_{BG})	$\frac{1-\cos r}{2\pi} C(\kappa_{BG}) \exp[-\kappa_{BG}^2 r^2/2]$
[e]Lorentzian ($\lambda = \lambda(\kappa_L)$)	$\frac{1-\cos r}{2\pi}(1+\lambda) \frac{(1+2\lambda)^2 + 4\lambda(\lambda+1)\cos^2(r/2)}{[(1+2\lambda)^2 - 4\lambda(\lambda+1)\cos^2(r/2)]^2}$
[f]Isotropic Gaussian (κ_{IG})	$\frac{1-\cos r}{2\pi} \sum_{m=0}^{\infty} (2m+1) \exp[-m(m+1)/(2\kappa_{IG}^2)] \frac{\sin[(m+1/2)r]}{\sin(r/2)}$
Wrapped Trivariate Normal (κ)	$\sum_{m=-\infty}^{\infty} \frac{\kappa^3}{\sqrt{2\pi}} (2m\pi - r)^2 \exp[-\kappa^2 (2m\pi - r)^2/2]$

[a]León et al. 2006, sec. 5.2; [b]Schaeben, 1997 (while not noted previously, these are the same).
[c]Downs, 1972; Khatri & Mardia, 1977; Matthies et al., 1988; León et al. 2006, sec. 5.2.
[d]Bunge, 1982; Matthies et al., 1988; Bucharova & Savyolova, 1993.
[e]Matthies, 1982; Matthies et al., 1988.
[f]Savyolova, 1984; Matthies et al., 1988; Nikolayev & Savyolova, 1997; Borovkov & Savyolova, 2007.

with mean rotation $\mathbf{S}$ and the density of the wrapped angle $r = t(\text{mod}2\pi)$ being

$$g(r) = \sum_{m=-\infty}^{\infty} \tilde{g}(r + m2\pi), \quad r \in (-\pi, \pi], \tag{3}$$

on the unit circle S^1; this is relevant for the wrapped trivariate normal distribution (wTND) described in Section 3.1. Further, any random orientation $\mathbf{O}$ having a density (1) on $SO(3)$ with respect to the uniform distribution, which depends on $\mathbf{O}$ only through a function $h[tr(\mathbf{O})]$, has UARS distribution with mean rotation $\mathbf{I}_3$ and an angle r with Lebesgue density $h[1 + 2\cos r](1 - \cos r)/(2\pi)$ on $r \in (-\pi, \pi]$ (i.e., the density for $\mathbf{O}$ is zonal/central on $SO(3)$ in that $h[tr(\mathbf{O})] = h\left[tr(\mathbf{O}_1^T\mathbf{O}\mathbf{O}_1)\right]$ for $\mathbf{O}, \mathbf{O}_1 \in SO(3)$, cf. Hielscher, 2010). If $\mathbf{v}$ has an isotropic (rotation-invariant or spherically symmetric) distribution on $\mathbb{R}^3$, then $\exp(\mathbf{A}(\mathbf{v}))$ has a UARS distribution (where the distribution of the angle $\|\mathbf{v}\|$ need not be continuous) and any UARS can be obtained this way. Finally, as quaternions (vectors on S^3, the $\mathbb{R}^4$ unit sphere) can be equivalently used to represent rotations, if $\mathbf{u} = (u_1, u_2, u_3)^T$ and r denote the random Euler axis-angle in the UARS formulation (1), then the Cayley-Klein map $\rho(\mathbf{w}) = \mathbf{I}_3 + 2w_1\mathbf{A}((w_2, w_3, w_4)^T) + 2\mathbf{A}((w_2, w_3, w_4)^T)^2$ of the random quaternion $\mathbf{w} = (w_1, w_2, w_3, w_4)^T = (u_1 \sin(r/2), u_2 \sin(r/2), u_3 \sin(r/2), \cos(r/2))^T$ has a UARS distribution on $SO(3)$ with mean rotation $\mathbf{I}_3$, and all distributions on quaternions which are rotationally symmetric about $(0, 0, 0, 1)^T$ induce UARS distributions on $SO(3)$ through this mapping (cf. Watson, 1983; Prentice, 1986; Schaeben & Nikolayev (1998, p. 66); Mardia and Jupp, 2000, p. 285). For more on UARS distributions and map-induced distributions on $SO(3)$ (via the exponential matrix on $SO(3)$ or Cayley-Klein map on S^3) see Jupp & Mardia (2000, p. 179, ch. 13.2), León et al. (2006, sec. 5.2), Bingham et al. (2009a) and Hielscher et al. (2010).

2.2 A CLT Motivation for the IGD on $SO(3)$

In reviewing (and partially criticizing) several UARS models on $SO(3)$ used in texture analysis, including Bunge's Gaussian, the Lorentzian and the isotropic Matrix Fisher distributions (cf. Table 1), Matthies et al. (1988, p. 85) argued that it may be physically plausible to imagine crystal orientations observed in materials as built from composition of small, inde-

pendent rotations in the texture development and therefore reasonable to motivate a "normal" distribution for orientation data by a CLT for rotations. Those authors informally provided a density on $SO(3)$ for the limit distribution of rotational compositions, and Savyolova (1984) derived the same density by characterizing a "normally" distributed rotation as having an infinitely divisible distribution. This density corresponds to the isotropic Gaussian distribution (IGD) on $SO(3)$ (see Table 1), which has been further studied and generalized by Nikolayev & Savjolova (1997) and also has direct connections to the Brownian motion distribution on upper 4-D hyperspheres (cf. Schaeben, 1992, Sec. 4). Schaeben (1992) and Schaeben & Nikolayev (1998, sec. 5) criticized the work of Matthies et al. (1988), arguing that no physically meaningful CLT argument for rotations could motivate the IGD as "normal" on $SO(3)$ and that no CLT analog exists for compositions in $SO(3)$ under assumptions similar to those for the CLT in Euclidean spaces. But this is untrue, as seen in Proposition 1, which straightforwardly combines a CLT result of Parthasarathy (1964) on $SO(3)$ with a triangular array of UARS-distributed rotations (see the Supplementary Material for details).

Proposition 1 *Suppose $r_{1,n}, \ldots, r_{n,n}$ are iid draws from a symmetric distribution on $(-\pi, \pi]$ with variance $\sigma^2 > 0$ and, independently, let $\mathbf{u}_{1,n}, \ldots, \mathbf{u}_{n,n}$ be iid vectors, uniformly distributed on S^2. Fix $\mathbf{S} \in SO(3)$ and define UARS rotations $\mathbf{O}_{1,n}, \ldots, \mathbf{O}_{n,n}$ by forming $\mathbf{O}_{i,n}$ with angle $r_{i,n}/\sqrt{n}$ and axis $\mathbf{u}_{i,n}$ in (1). Then, the composition $\mathbf{O}^{(n)} = \mathbf{S} \prod_{i=1}^{n} \mathbf{O}_{i,n}$ converges in distribution to an isotropic Gaussian distribution on $SO(3)$ as $n \to \infty$, a UARS model with mean rotation $\mathbf{S}$ and angular density in Table 1 having concentration parameter $\kappa_N = \sqrt{3}/\sigma$.*

Hence, the IGD on $SO(3)$ does indeed have a CLT-motivation as the limit of several "small" iid physical rotations in 3-D, supporting the argument of Matthies et al. (1988) that this distribution can provide a plausible description of the overall results from the operation of small random rotational effects. Beyond Proposition 1, the composition of independent UARS-distributed rotations will always be UARS-distributed and, hence, the UARS class of distributions is closed under composition; see the Supplementary Material. But more is true for the IGD on $SO(3)$, because the convolution of independent rotations with an IGD will again have an IGD (cf. Theorem 3, Nikolayev & Savjolova, 1997). In these ways, the IGD on

$SO(3)$ does behave like a "normal" distribution typically associated with any Euclidean space, which partly explains its appeal for modeling orientation data.

The IGD on $SO(3)$ is again characterized by an angular density (cf. Table 1) in (1) which is not particularly tractable. Other angular densities with analytically simpler forms, like those associated with the Bunge's Gaussian and the isotropic Matrix Fisher distributions on $SO(3)$, have been suggested as approximations for the IGD (cf. Nikolayev & Savjolova, 1997). But these have also been criticized as having shortcomings (cf. Matthies et al., 1988; Bucharova & Savylova, 1992). For example, the normalizing constant in the angular density for Bunge's Gaussian distribution is not expressible in a closed form (Bucharova & Savylova, 1992 and Table 1 here), and the Matrix Fisher-based approximation is not good except for very large concentrations (see Section 3.2 and Figure 2). This motivates us to consider a wrapped trivariate normal distribution (wTND) to provide a simple distributional approximation to the IGD on $SO(3)$ in Section 3.

Before leaving this section, we add that the criticism by Schaeben (1992) and Schaeben and Nikolayev (1998) mentioned above largely concerned an operational definition of a "normal" distribution on $SO(3)$. As with the normal distribution on $\mathbb{R}$, various characterizations of "normality" exist for rotations. For example, Bunge's (1982) Gaussian distribution is an analog of the real-valued normal distribution in terms of being a solution to a diffusion equation (i.e., heat equation) on manifolds (cf. Table 1; Bucharova and Savylova, 1992; Chirikjian, 2009, sec. 2.1.5). Schaeben (1992) commented that, statistically speaking, the isotropic Matrix Fisher distribution could be argued to be "normal" due to its matrix density representation (1),

$$f(\mathbf{O}|\mathbf{S},\kappa) = \exp[\kappa_F^2 2^{-1}(tr(\mathbf{S}^T\mathbf{O}) - 1)]/[I_0(\kappa_F^2) - I_1(\kappa_F^2)], \quad \mathbf{O} \in SO(3),$$

which has an exponential form, decaying away from its mode $\mathbf{S}$ (as does a normal distribution in Euclidean space). While a valid point, on the other hand the Matrix Fisher rotational distribution is itself not the limit distribution of small rotational compositions, and this family is also not closed under convolutions (Schaeben & Nikolayev, 1998, p. 78), making the Matrix Fisher model for rotations less "normal" in these senses than the IGD on $SO(3)$ described

above. As Schaeben & Nikolayev (1998) also noted, the isotropic Matrix Fisher distribution closely matches the IGD on $SO(3)$ (or related Brownian motion on the 4-D hypersphere) for highly concentrated orientations, which has close connections to results for directional data on the $\mathbb{R}^p$-unit sphere S^{p-1}. Roberts & Ursell (1960) (for $p = 3$) and Kent (1978) provided close bounds on the densities of von Mises-Fisher and Brownian motion distributions on S^{p-1} for large concentration parameters, and Hartman & Watson (1974) showed that the von Mises-Fisher distribution on S^{p-1} can be expressed as a mixture of Brownian motion distributions on S^{p-1} (cf. Jupp & Mardia, 2000, p. 173). While also true, for *any* concentrated UARS distribution with continuously differentiable density and mean rotation $\mathbf{I}_3$, a Taylor expansion of the density about $\mathbf{I}_3$ shows that it is close to that of an IGD on $SO(3)$ (as a referee has pointed out). And compared to the Matrix Fisher and other UARS models, the wTND of the next section can provide closer approximations to the IGD on $SO(3)$ for a wider range of concentration parameters.

3 Wrapped Trivariate Normal Distributions on $SO(3)$

3.1 Definition and Motivation

Suppose $\mathbf{X}$ has a trivariate normal distribution $N(\mathbf{0}_3, \kappa^{-2}\mathbf{I}_3)$ on $\mathbb{R}^3$ with component variance $\kappa^{-2} > 0$. Then, by wrapping $\mathbb{R}^3$ onto $SO(3)$ as in Section 2.1, $\mathbf{S}\exp[\mathbf{A}(\mathbf{X})]$ defines a wrapped trivariate normal distribution (wTND) on orientations with (fixed) mean rotation $\mathbf{S} \in SO(3)$ and concentration parameter $\kappa > 0$. For a random variable b independent of $\mathbf{X}$ with $P(b = 1) = P(b = -1) = 1/2$, one may decompose $\mathbf{X} = \mathbf{tu}$ in terms of independent $t = b\|\mathbf{X}\|$ and $\mathbf{u} = b\mathbf{X}/\|\mathbf{X}\|$, where $\mathbf{u}$ is uniformly distributed on S^2, to see that the wTND is a UARS model with an angle-axis construction (1) defined by $\mathbf{u}$ and $r = t(\mathrm{mod}2\pi)$. As $\kappa^2 t^2$ has chi-square distribution χ^2_3 with 3 degrees of freedom, it follows from (3) that a random "spin" or angle $r \in (-\pi, \pi]$ has a (Lebesgue) density

$$g_{wTN}(r|\kappa) = \frac{\kappa^3}{\sqrt{2\pi}} \sum_{m=-\infty}^{\infty} (2m\pi - r)^2 \exp(-\kappa^2(2m\pi - r)^2/2) \tag{4}$$

corresponding to a wrapped (symmetrized) Maxwell-Boltzmann distribution with concentration parameter $\kappa > 0$ (up to scaling, the Maxwell-Boltzmann distribution is that of the square-root of a χ^2_3 variable and appears in modeling particle speeds in statistical mechanics, cf. Peckham & McNaught, 1992). The wrapped kernel in (4) closely resembles that of the wrapped normal density on $(-\pi, \pi]$,

$$g(r|\delta) = \frac{1}{\sqrt{2\pi}\delta} \sum_{m=-\infty}^{\infty} \exp(-(2m\pi - r)^2/2\delta^2), \quad r \in (-\pi, \pi]$$

which is a commonly used angular distribution for modeling for 2-D rotations (with standard deviation parameter $\delta > 0$). However, unlike the wrapped normal, the angular density (4) is bimodal and converges to a symmetrized small-variance Maxwell-Boltzmann distribution as the wrapping becomes effectively inconsequential (e.g., as $\kappa \to \infty$).

The wTND has a CLT-motivation in $\mathbb{R}^3$. That is, sums of iid small variance quantities in $\mathbb{R}^3$ lead to trivariate normal distributions in Euclidean space which can then be wrapped onto $SO(3)$. In particular, defining $\mathbf{s}_n = \sum_{i=1}^n r_{i,n}\mathbf{u}_{i,n}$ with iid $\mathbf{u}_{1,n}, \ldots, \mathbf{u}_{n,n}$ uniformly-distributed on S^2 and iid random angles $r_{1,n}, \ldots, r_{n,n}$ from a common distribution on $(-\pi, \pi]$ having mean zero and variance σ^2/n for some $\sigma > 0$, $\exp[\mathbf{A}(\mathbf{s}_n)]$ converges to wTND on $SO(3)$ with mean rotation $\mathbf{I}_3$ and $\kappa = \sqrt{3}/\sigma$ by the usual CLT in $\mathbb{R}^3$. As $\exp[\mathbf{A}(\mathbf{s}_n)] \approx \prod_{i=1}^n \mathbf{M}(r_{i,n}, \mathbf{u}_{i,n})$ for small rotations in (1), the wTND also approximates the IGD on $SO(3)$ as the limit of a large number of compositions of "small" independent random rotations (cf. Proposition 1), a phenomenon which is next investigated through simulation.

3.2 Comparisons of the wTND to Other UARS Models

One expects the wTND (and other UARS models) to be close to the IGD on $SO(3)$ for sufficiently large concentrations κ. To gain some rough idea of how large κ must be for effective approximations, in Figure 1 we plot the cumulative distribution functions of $|r|$ for a random angle $r \in (-\pi, \pi]$ from the symmetric angular density (4) of the wTND as well as the angular density from the IGD on $SO(3)$ with concentrations $\kappa = 3, 2, 1, 0.5$ (cf. Table 1), and we compare these against the true sampling distribution of the absolute angle $|r_n|$ result-

ing from the composition of n iid rotation matrices $\mathbf{M}(r_{i,n}, \mathbf{u}_{i,n})$ with the angles $r_{i,n}$ having uniform$(-3\kappa^{-1}n^{-1/2}, 3\kappa^{-1}n^{-1/2})$ distributions for $n = 4, 10$. The comparisons show that at least when $\kappa \geq 2$, the wTND effectively approximates the IGD's angular distribution, which is in turn a good approximation to the real angular distribution that describes the composition. The central limit convergence of products to a IGD limit appears to be remarkably fast, suggesting potentially wide-spread applications for the family (and good approximations to it) where observed physical orientations are plausibly modeled as derived from multiple small random perturbations of a basic orientation.

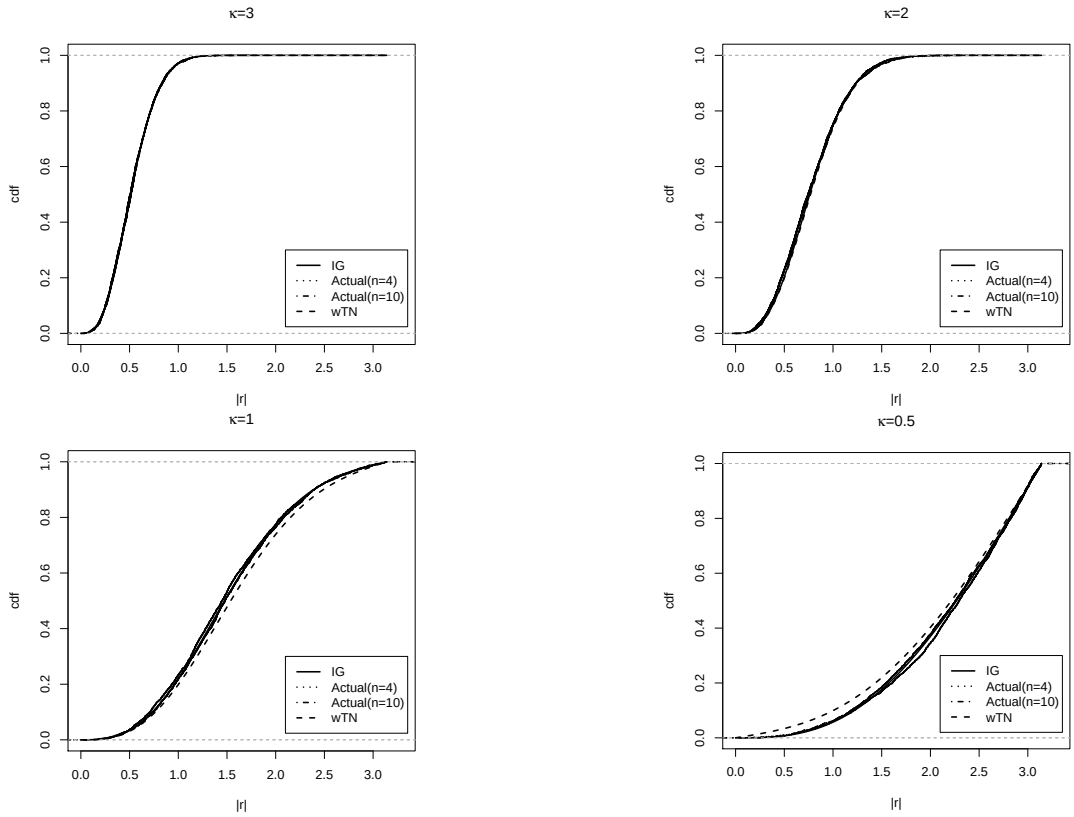

Figure 1 Cumulative distribution functions (cdfs) of $|r|$ for angles $r \in (-\pi, \pi]$ from the symmetric angular densities associated with isotropic Gaussian (IG) or wrapped trivariate normal (wTN) distributions on $SO(3)$ with different concentration parameters $\kappa > 0$. Also provided are the actual cdfs of the absolute angle $|r_n|$ (approximated from 100,000 simulations) as determined by the product of $n = 4, 10$ independent UARS-distributed rotation matrices (each having uniform$(-3\kappa^{-1}n^{-1/2}, 3\kappa^{-1}n^{-1/2})$ angular distributions).

As mentioned in Sections 1 and 2, common rotational models belong to the UARS class and so can be described in terms of their angular densities, listed in Table 1 (an alternative description of UARS distributions through related densities is described in the Supplementary Material). Where necessary, we have reparameterized the densities from their most common forms so that all parameters κ are non-negative and control the concentrations of the distributions in a similar manner. Except for the Lorentzian case, the angular densities for the models in Table 1 will again be nearly identical (i.e., matching that of the IGD) if the parameters κ are large enough. In Figure 2, we also compare the (absolute) angular densities from Table 1 for the isotropic Cayley (i.e., de la Vallée Poussin distribution), Matrix Fisher, Bunge's Gaussian and wTN models to that of the IGD on $SO(3)$ for $\kappa = 10, 5, 2, 1$. From the graphs, we can see that the (absolute) angular density from the wTND approximates the (absolute) angular density of the IGD much better than the Cayley and Matrix Fisher-distributions, and at least as well as Bunge's Gaussian distribution when κ is small (though, as indicated in Table 1, the angular density from the wTND has a closed form while normalizing constant of Bunge's Gaussian distribution has to be numerically determined for each concentration parameter κ in Figure 2).

We end this section by noting that the wTND, perhaps unlike other angular densities in Table 1, has a particularly direct and simple path to simulation which can be attractive for modelers, especially for large concentration parameters. One may either simulate (and wrap) independent $N(0, \kappa^{-2})$ values, or simulate a random angle from the wTN angular density (4) for use in (1) via $r = (-1)^b|\kappa^{-1}w^{1/2} - \pi\lfloor\kappa^{-1}w^{1/2}/\pi\rfloor|$ with χ^2_3 random variable w and an independent Bernoulli variable b (0 or 1 with equal probabilities).

4 One-Sample Bayes Methods for wTND on $SO(3)$

From the angular density (4), we obtain the density (with respect to the uniform distribution) for wTND on $SO(3)$ as

$$f(\mathbf{O}|\mathbf{S}, \kappa) = \frac{4\pi}{3 - tr(\mathbf{S}^T\mathbf{O})} g_{wTN}(\arccos[2^{-1}(tr(\mathbf{S}^T\mathbf{O}) - 1)]|\kappa), \quad \mathbf{O} \in SO(3) \tag{5}$$

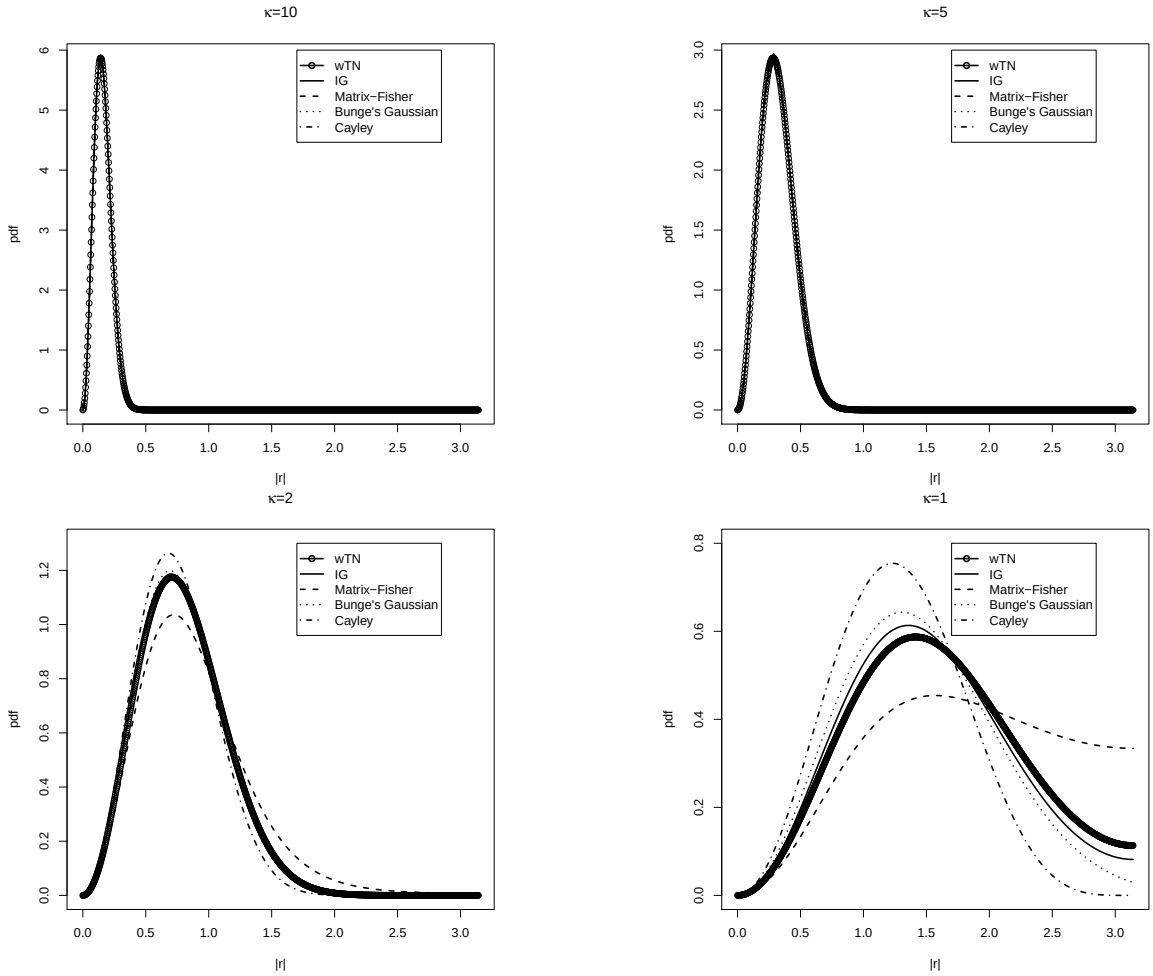

Figure 2 Absolute angular densities (i.e., densities for $|r|$) when $r \in (-\pi, \pi]$ follows the symmetric angular density associated with the isotropic Gaussian (IG), wrapped trivariate normal (wTN), isotropic Matrix Fisher, isotropic Cayley, or Bunge's Gaussian rotational distributions.

from (1). The density (5) has a singularity at $\mathbf{O} = \mathbf{S}$. (The other models represented in Table 1 do not have such singularities due to the term $1 - \cos r$ in their densities for r.) However, this fact does not prevent us from developing useful Bayes inference, where maximum likelihood estimation would technically be undefined. In fact, due to the non-regularity of the likelihood function, the convergence rate of Bayes procedures for estimating $\mathbf{S}$ can be *super-efficient* and observably so in realistic sample sizes for small κ, as we will illustrate with simulations in Section 5. At the same time, for sufficiently large concentration parameters κ, the wTND can also behave "regularly" whereby the numerator of its matrix density (5) decays to zero rapidly

enough to effectively cancel out the singularity; the simulations of Section 5 will also clarify this behavior.

For Bayes inference, we would like to identify potentially non-informative prior distributions for the parameters $\mathbf{S}$ and κ of the wTND$(\mathbf{S}, \kappa)$, so that the resulting credible regions have good frequentist coverage properties. To this end, we use a prior selection approach as in the Bayes methods of Bingham et al. (2009bc).

As a prior for the mean rotation parameter $\mathbf{S}$, we use the uniform distribution on $SO(3)$ having density $p(\mathbf{S}) = 1$, $\mathbf{S} \in SO(3)$. For the concentration parameter κ, we use the Jeffreys prior for the angular density. It is slightly more convenient for discussion and plotting purposes to consider the corresponding prior for the spread parameter $\eta = -\log \kappa$ which has density

$$J(\eta) = \exp(-\eta)\sqrt{\mathcal{I}(\exp(-\eta))}, \quad \eta \in (-\infty, \infty)$$

for

$$\begin{aligned} \mathcal{I}(\kappa) &= \mathrm{E}\left[\left(\frac{d}{d\kappa}\log g_{wTN}(r|\kappa)\right)^2\right] \\ &= -\frac{9}{\kappa^2} + \frac{\kappa^5}{\sqrt{2\pi}}\int_{-\pi}^{\pi} \frac{\left(\sum_{m=-\infty}^{\infty}(2m\pi - r)^4 \exp(-\kappa^2(2m\pi - r)^2/2)\right)^2}{\sum_{m=-\infty}^{\infty}(2m\pi - r)^2 \exp(-\kappa^2(2m\pi - r)^2/2)} dr. \end{aligned}$$

While this density does not have a closed form, $J(\eta)$ can be evaluated numerically and we display this (improper) Jeffreys prior density in Figure 3. It holds that $J(\eta) \to 0$ as $\eta \to \infty$ and $J(\eta) \to \sqrt{6}$ as $\eta \to -\infty$ so that, to determine $J(\eta)$ numerically in simulations to follow, we use $J(\eta) \approx \sqrt{6}$ when $\eta < -0.5$, $J(\eta) \approx 0$ when $\eta > 2$ and, for $-0.5 \leq \eta \leq 2$, we fit a cubic spline to approximate $J(\eta)$ after calculating the density at grid points $-0.5 + 2.5/1000 \cdot i$, $i = 0, 1, \ldots, 1000$.

From Figure 3, we see that the Jeffreys prior density, perhaps surprisingly, is not a simple monotone or unimodal function and has turning points around $\eta = 0.5$ and $\eta = 0.85$. The non-monotonicity affects the behavior of samples simulated from the posterior distribution, especially for small sample sizes, which we will note later in Section 5.

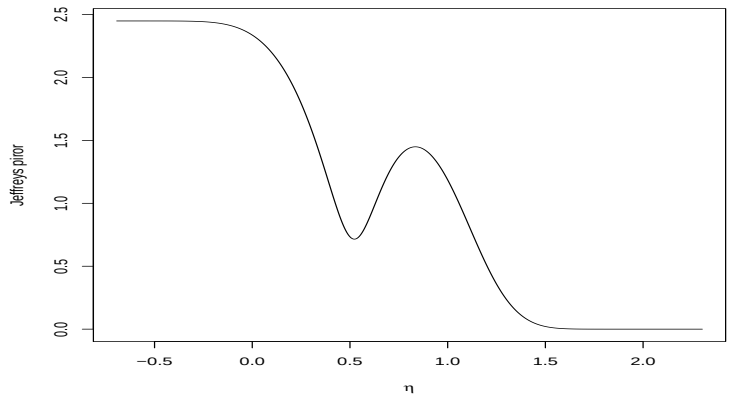

Figure 3 (Improper) Jeffreys prior density for $\eta = -\log \kappa$.

With respect to a random sample $\mathbf{O}_i$, $i = 1, ..., n$ from the wTND, the corresponding likelihood function for $(\mathbf{S}, \eta)$ is

$$L(\mathbf{S}, \eta) \propto \frac{\prod_{i=1}^{n} g_{wTN}(\arccos[2^{-1}(tr(\mathbf{S}^T\mathbf{O}_i) - 1)]| \exp(-\eta))}{\prod_{i=1}^{n}(3 - tr(\mathbf{S}^T\mathbf{O}_i))}$$

by (5). Multiplying by prior densities $p(\mathbf{S})$ and $J(\eta)$ gives a posterior density $h(\mathbf{S}, \eta)$ for $(\mathbf{S}, \eta)$ proportional to

$$\left(\frac{\prod_{i=1}^{n} g_{wTN}(\arccos[2^{-1}(tr(\mathbf{S}^T\mathbf{O}_i) - 1)]| \exp(-\eta))}{\prod_{i=1}^{n}(3 - tr(\mathbf{S}^T\mathbf{O}_i))} \right) J(\eta).$$

We sample a sequence $(\mathbf{S}^j, \eta^j)$ from the posterior distribution using a Metropolis-Hastings-within-Gibbs (MHG) algorithm as follows. With variables $\mathbf{O}_1, ..., \mathbf{O}_n \in SO(3)$ and the starting values $\mathbf{S}^0, \eta^0$:

1. As a proposal for $\mathbf{S}^j$, generate $\mathbf{S}^{j^*}$ from the isotropic Matrix Fisher distribution with location parameter $\mathbf{S}^{j-1}$ and concentration κ_F (i.e., use the angular density in Table 1 in (1)). (Here κ_F is a tuning parameter.)

2. Compute $r_j^{(1)} = \frac{h(\mathbf{S}^{j^*}, \eta^{j-1})}{h(\mathbf{S}^{j-1}, \eta^{j-1})}$ and generate $w_j^{(1)} \sim$ Bernoulli$(\min(1, r_j^{(1)}))$. Take $\mathbf{S}^j =$

$w_j^{(1)}\mathbf{S}^{j^*} + (1 - w_j^{(1)})\mathbf{S}^{j-1}$.

3. Generate normal $\eta^{j^*} \sim N(\eta^{j-1}, \gamma^2)$. (Here γ is a tuning parameter.)

4. Compute $r_j^{(2)} = \frac{h(\mathbf{S}^j, \eta^{j^*})}{h(\mathbf{S}^j, \eta^{j-1})}$ and generate $w_j^{(2)} \sim$ Bernoulli$(\min(1, r_j^{(2)}))$. Take $\eta^j = w_j^{(2)}\eta^{j^*} + (1 - w_j^{(2)})\eta^{j-1}$.

Section 5 next describes a simulation study of one-sample Bayes inference for the wTND using this algorithm (considering various values of η and sample sizes n), and we explain how posterior draws can be used to construct credible regions for $\mathbf{S} \in SO(3)$ and $\eta \in \mathbb{R}$. We also provide the coverage probabilities and sizes of the resulting credible regions to demonstrate the effectiveness of the Bayes methods for the wTN model.

5 Bayes Credible Regions and Coverage Accuracy

We conducted a simulation study for several different combinations (n, η). In generating rotation data from the wTND$(\mathbf{S}, \kappa = \exp[-\eta])$, we set the true mean rotation $\mathbf{S}$ to be $\mathbf{I}_3$, as the choice of $\mathbf{S}$ is irrelevant (cf. Bingham et al. 2009a). The values used for the parameter η (on the spread-scale) were $-3.454, -1.844, -1.151, -0.347, 0, 0.5, 0.85, 1.3$ and sample sizes were $n = 10, 30, 100, 300, 1000$.

For each combination (n, η), we simulated 4000 data sets, each a random sample of size n from the wTND. For each data set, we generated $N = 100,000$ samples from the posterior distribution using the MHG algorithm after a $25,000$ iteration burn-in period. After inspecting several different starting values and finding the simulation results to be insensitive to this choice, we chose starting values for $\mathbf{S}^0$ and η^0 in the simulation study to be the true parameters. The tuning parameters κ_F and γ listed in Table 2 were chosen to keep the Metropolis-Hastings jumping rates between 30% and 40%.

For the purpose of analysis, a 95% credible level was used. Two types of credible intervals for η were obtained from the posterior sampling, equal-tail (ET) intervals and shortest length (SL) intervals. Credible regions for $\mathbf{S}$ were constructed using the method of "credible sets of cones" described by Bingham et al. (2009c). That is, if $\mathbf{S}^1, \ldots, \mathbf{S}^N$ denote the posterior samples,

Table 2 Values of tuning parameters $\kappa_F = \sqrt{2\rho}$ and γ expressed in terms of (ρ, γ).

	$n = 10$		$n = 30$		$n = 100$		$n = 300$		$n = 1000$	
	ρ	γ	ρ	γ	ρ	γ	ρ	γ	ρ	γ
$\eta = 1.3$	5	0.5	50	0.5	1000	0.4	5000	0.3	200000	0.25
$\eta = 0.85$	1	0.7	10	0.5	200	0.2	1500	0.15	4000	0.08
$\eta = 0.5$	0.5	0.7	0.7	0.5	2	0.3	4	0.2	20	0.1
$\eta = 0$	2	0.7	4	0.5	15	0.13	50	0.08	200	0.05
$\eta = -0.347$	5	0.4	20	0.23	50	0.13	150	0.07	500	0.04
$\eta = -1.151$	33	0.4	100	0.23	350	0.13	800	0.07	3000	0.04
$\eta = -1.844$	150	0.4	300	0.23	1200	0.13	4000	0.07	12000	0.04
$\eta = -3.454$	4000	0.4	10000	0.23	35000	0.13	80000	0.07	300000	0.04

we define a Bayes point estimate $\mathbf{S}_B$ of the mean rotation as the maximizer of $\sum_{j=1}^{N} tr(\mathbf{S}_B^T \mathbf{S}^j)$ (i.e., the Bayes estimator under a squared error loss function $tr[(\mathbf{S}_B - S)(\mathbf{S}_B - S)^T]$), and then define a credible region by a "set of cones" of angle a around each column vector in $\mathbf{S}_B$, where a is the 95th percentile of $\{a_1, \ldots, a_N\}$ and each a_j represents the maximum arccosine value (between 0 and π) of the diagonal elements of $\mathbf{S}_B^T \mathbf{S}^j$. Hence, a region for $\mathbf{S}$ can be graphically illustrated as in Figure 4 and the size of the region is defined in terms of the angle between the centers (columns of $\mathbf{S}_B$) and edges of the cones.

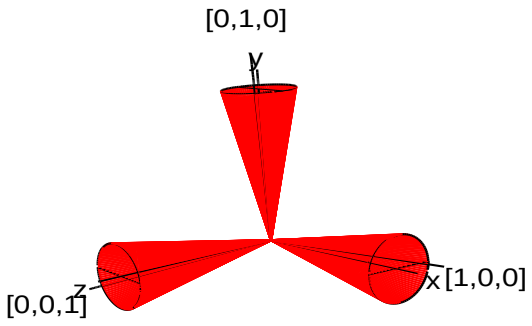

Figure 4 A 95% credible region for the parameter $\mathbf{S}$ with x, y and z representing the orientation (i.e., column vectors) of the Bayes point estimate $\mathbf{S}_B = [x\, y\, z]$ for $\mathbf{S}$.

After finding the credible regions for $\mathbf{S}$ and η for each of the 4000 data sets at each (n, η), we determined whether the regions for $\mathbf{S}$ and η contained the true values. This provided

the coverage rates for $\mathbf{S}$ and η for the (n, η) combinations in Table 3. For both $\mathbf{S}$ and η, the frequentist coverage rates of Bayes regions are consistent with their credible levels and as sample size increases, the coverage rates converge to the nominal ones. This indicates that the current Bayes approach is effective for obtaining good frequentist coverage accuracy.

Table 3 Coverage rates (%) for $\boldsymbol{S}$ and η using 95% Bayes credible regions for different combinations of (n, η); credible regions for η characterized here are ET intervals (with SL intervals performing similarly).

(n, η)	$\mathbf{S}$	η	(n, η)	$\mathbf{S}$	η
$(10, 1.3)$	95.5	95.6	$(10, -0.347)$	96.0	95.9
$(30, 1.3)$	95.9	93.9	$(30, -0.347)$	95.4	94.6
$(100, 1.3)$	92.9	94.9	$(100, -0.347)$	95.0	96.0
$(300, 1.3)$	95.2	95.4	$(300, -0.347)$	96.3	96.2
$(1000, 1.3)$	95.2	94.9	$(1000, -0.347)$	95.2	95.0
$(10, 0.85)$	93.2	98.6	$(10, -1.151)$	95.5	94.6
$(30, 0.85)$	95.9	98.2	$(30, -1.151)$	93.2	95.5
$(100, 0.85)$	95.1	95.5	$(100, -1.151)$	93.1	96.0
$(300, 0.85)$	94.9	94.5	$(300, -1.151)$	94.2	94.1
$(1000, 0.85)$	95.0	95.1	$(1000, -1.151)$	95.0	94.6
$(10, 0.5)$	93.5	96.4	$(10, -1.844)$	97.3	95.9
$(30, 0.5)$	96.7	95.6	$(30, -1.844)$	93.6	93.6
$(100, 0.5)$	95.3	95.2	$(100, -1.844)$	94.3	94.3
$(300, 0.5)$	94.7	94.9	$(300, -1.844)$	95.3	94.0
$(1000, 0.5)$	95.1	95.3	$(1000, -1.844)$	95.0	95.4
$(10, 0)$	95.9	94.4	$(10, -3.454)$	94.7	95.4
$(30, 0)$	95.5	95.9	$(30, -3.454)$	95.0	95.5
$(100, 0)$	95.5	92.7	$(100, -3.454)$	93.1	95.0
$(300, 0)$	94.7	93.9	$(300, -3.454)$	95.4	95.1
$(1000, 0)$	95.2	95.0	$(1000, -3.454)$	95.0	94.9

We also considered median sizes for the 4000 credible regions for $\mathbf{S}$ and η, where we used the cone angle to characterize the size of a region for $\mathbf{S}$ and computed lengths of both ET and SL credible intervals for η. Results are summarized in Tables 4 and 5.

From Table 4, the two methods for obtaining 95% intervals for η produce similar results for all combinations (n, η). Also, for fixed η, as sample size n increases, the intervals become narrower. It is reasonable that with more data, the estimation of η is more precise. For fixed n, the width of interval for η is not strictly monotone decreasing in η due to the effect of the prior shape. For small η (which means large concentration parameter κ), especially for $\eta < 0$ (i.e. $\kappa > 1$), the width does not change as η changes.

As seen in Table 5, for fixed η, the median angle decreases as n increases. For each $\eta > 0$,

Table 4 Median width of 95% Bayes credible intervals for η with different combinations of (n, η) and both equal-tail (ET) and shortest-length (SL) intervals.

(n,η)	ET Width	SL Width	(n,η)	ET Width	SL Width
(10,1.3)	1.429	1.405	$(10,-0.347)$	0.559	0.554
(30,1.3)	0.574	0.566	$(30,-0.347)$	0.300	0.298
(100,1.3)	0.432	0.428	$(100,-0.347)$	0.161	0.160
(300,1.3)	0.351	0.348	$(300,-0.347)$	0.093	0.092
(1000,1.3)	0.282	0.276	$(1000,-0.347)$	0.051	0.051
$(10,0.85)$	1.275	1.252	$(10,-1.151)$	0.543	0.538
$(30,0.85)$	0.895	0.870	$(30,-1.151)$	0.299	0.297
$(100,0.85)$	0.330	0.322	$(100,-1.151)$	0.161	0.160
$(300,0.85)$	0.161	0.160	$(300,-1.151)$	0.093	0.092
$(1000,0.85)$	0.086	0.086	$(1000,-1.151)$	0.051	0.051
$(10,0.5)$	1.210	1.192	$(10,-1.844)$	0.543	0.538
$(30,0.5)$	0.787	0.781	$(30,-1.844)$	0.298	0.297
$(100,0.5)$	0.470	0.469	$(100,-1.844)$	0.161	0.160
$(300,0.5)$	0.313	0.307	$(300,-1.844)$	0.092	0.092
$(1000,0.5)$	0.157	0.153	$(1000,-1.844)$	0.051	0.050
$(10,0)$	1.370	1.322	$(10,-3.454)$	0.542	0.538
$(30,0)$	0.358	0.347	$(30,-3.454)$	0.298	0.297
$(100,0)$	0.171	0.170	$(100,-3.454)$	0.161	0.160
$(300,0)$	0.098	0.097	$(300,-3.454)$	0.092	0.092
$(1000,0)$	0.053	0.053	$(1000,-3.454)$	0.051	0.050

the empirical convergence rate (found by regressing the log of median angle over the log of n for $n = 100, 300, 1000$) is approximately $O(1/n)$ due to the non-regularity of the likelihood (cf. a circular data case in Nordman et al. 2009). But for small η where $\eta \leq 0$, the empirical convergence rate is approximately $O(1/\sqrt{n})$. This is consistent with our claim that for large concentration parameter κ, the wTND effectively approximates the IGD on $SO(3)$ (which has regular behavior). In other words, for large κ, there is effectively no wrapping involved in the angular density (4) from the wTND and so the only real contribution to the summation (4) is the $m = 0$ component, for which the r^2 term there will essentially behave like $1 - \cos r$. Intuitively, this $1 - \cos r$ factor allows the wTN density to "look like" angular densities in Table 1 corresponding to regular rotational distributions. Even for large concentrations, the wTN model is non-regular (due to the spikes in (5)) but, practically speaking, this aspect is not "seen" at even fairly large sample sizes.

Table 5 Median cone angle (in radians) of Bayes credible sets for **S** with different combinations (n, η) and the apparent moderate sample size convergence rate of the median angles for fixed η.

(n,η)	Angle	Apparent Convergence Rate	(n,η)	Angle	Apparent Convergence Rate
(10,1.3)	1.492		$(10,-0.347)$	0.667	
(30,1.3)	0.346		$(30,-0.347)$	0.390	
(100,1.3)	0.102	$n^{-1.008}$	$(100,-0.347)$	0.211	$n^{-0.505}$
(300,1.3)	0.031		$(300,-0.347)$	0.122	
(1000,1.3)	0.010		$(1000,-0.347)$	0.066	
$(10,0.85)$	1.542		$(10,-1.151)$	0.288	
$(30,0.85)$	1.503		$(30,-1.151)$	0.161	
$(100,0.85)$	0.243	$n^{-1.042}$	$(100,-1.151)$	0.088	$n^{-0.497}$
$(300,0.85)$	0.068		$(300,-1.151)$	0.050	
$(1000,0.85)$	0.022		$(1000,-1.151)$	0.028	
$(10,0.5)$	1.546		$(10,-1.844)$	0.141	
$(30,0.5)$	1.525		$(30,-1.844)$	0.080	
$(100,0.5)$	0.831	$n^{-0.920}$	$(100,-1.844)$	0.044	$n^{-0.499}$
$(300,0.5)$	0.153		$(300,-1.844)$	0.028	
$(1000,0.5)$	0.098		$(1000,-1.844)$	0.014	
$(10,0)$	1.485		$(10,-3.454)$	0.028	
$(30,0)$	0.725		$(30,-3.454)$	0.016	
$(100,0)$	0.371	$n^{-0.651}$	$(100,-3.454)$	0.009	$n^{-0.476}$
$(300,0)$	0.123		$(300,-3.454)$	0.005	
$(1000,0)$	0.082		$(1000,-3.454)$	0.003	

6 An Application to Orientation Data from EBSD

Here we make use of part of a data set collected in the study of Bingham et al. (2010). That paper provides details of an electron back-scatter diffraction (EBSD) experiment done to measure crystal orientations in a nickel specimen. Fourteen repeat scans were made on a 2-D rectangular grid on the specimen's planar surface, at over 4000 sites per scan. We use data from a particular 4×28 sub-grid and a single scan. The EBSD measurement device returned an orientation matrix (in terms of 3 Euler angles) at each location, and we consider the characterization of variation in orientations across the grid.

We used the Bayes methods in Bingham et al. (2009c) and this article to fit both isotropic Matrix Fisher and wTN models, respectively, to the 112 observed orientations. Although the computations involved were much more complicated, we also fit the IGD to the data by maximum likelihood. Estimated concentration parameters for these fits were respectively

$$\hat{\kappa}_F = 1.365, \quad \hat{\kappa} = 0.974, \text{ and } \hat{\kappa}_{IG} = 0.932.$$

In texture analysis, the absolute value $|r|$ of the random spin $r \in (-\pi, \pi]$ in a UARS rotation

(1) is often referred to as a misorientation angle (i.e., the smallest (non-negative) angle in an axis-angle representation needed to align a rotation (1) back to a standard reference frame $\mathbf{I}_3$, cf. Randall, 2003); note $|r|$ has a density on $[0, \pi]$ equaling twice the angular density (for r) listed in Table 1 for the isotropic Matrix Fisher distribution, the wTND, and the IGD. For each of these models, Figure 5 plots the fitted cumulative distribution function for the misorientation angle $|r|$. These are plotted against the empirical distribution $\{\widehat{|r|}_{ij} : i = 1, \ldots, 4; j = 1, \ldots, 28\}$ of misorientation angles, computed as $\widehat{|r|}_{ij} = \arccos\{[tr(\hat{\mathbf{S}}^T \boldsymbol{O}_{ij}) - 1]/2\}$ using a non-parametric "moment" estimator $\hat{\mathbf{S}}$ of the mean rotation for de-trending defined as the maximizer of $\sum_{i,j} tr(\boldsymbol{S}^T \boldsymbol{O}_{ij})$; this estimation of misorientation angles uses the fact that a UARS orientation $\mathbf{O} = \mathbf{S} \cdot \mathbf{M}(r, \mathbf{u})$ satisfies $tr(\mathbf{S}^T \mathbf{O}) = tr(\mathbf{M}(r, \mathbf{u})) = 1 + 2\cos|r|$ from (1).

The plot suggests that the fitted IGD and wTND are essentially identical, and do a better job of describing the "texture" of the nickel specimen in terms of variability in crystal orientations across this grid of locations (i.e., at this spatial resolution) than does the fitted Matrix Fisher model. The methods of this paper further establish that 95% cones for the mean rotation $\boldsymbol{S}$ in the wTND have angle 22.86° and that 95% limits for κ are 0.895 and 1.053. This example illustrates both the utility of the tractable wTN model and the methods of non-informative Bayes inference established in previous sections.

7 Conclusion

As one goal of the manuscript, we have provided a physical framework to motivate the isotropic Gaussian distribution (IGD) on $SO(3)$ as the limit distribution of a composition of large number of small, independent rotational errors (specifically, rotationally symmetric errors from the uniform-angle-random-spin (UARS) class of rotational distributions). This supports the argument that this distribution does act like a "normal" distribution for rotations (i.e., is motivated by CLT considerations) and therefore can provide a plausible description of small random effects operating in the development of orientation data, as suggested by Matthies et al. (1988) for material textures.

In part because the IGD has a complicated distributional form, this paper developed a

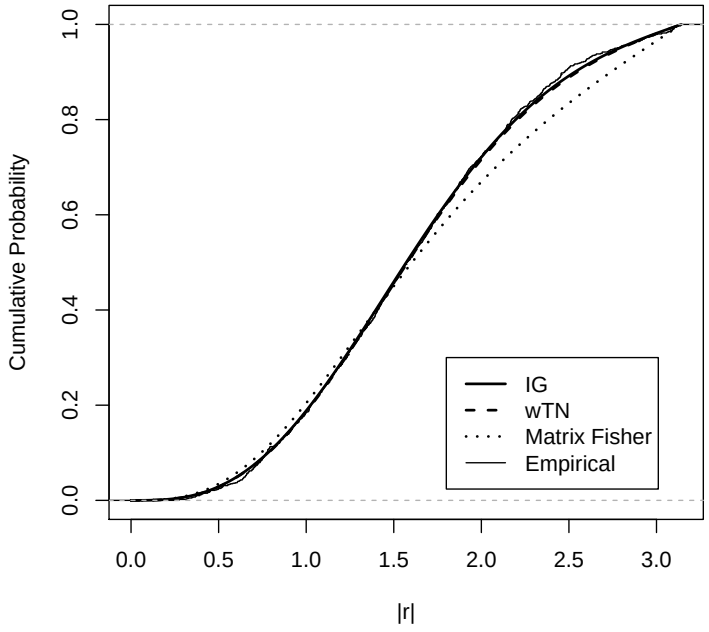

Figure 5 For the EBSD nickel data, plot of the empirical distribution of estimated misorientation angles and the cumulative distribution for $|r|$ in fitted models for the isotropic Matrix Fisher distribution, the wTND, and the IGD on $SO(3)$.

new UARS model as the wrapped trivariate normal distribution (wTND), which is tractable and provides natural approximations for the limit behavior of the composition of many small independent rotations. We have demonstrated the straightforward implementation and effectiveness of non-informative Bayes inference for these distributions, enabling their use as an attractive alternative to other UARS models for describing orientation data as random pertubations of a mean rotation parameter $\mathbf{S} \in SO(3)$.

There, of course, remains the question of conducting inference for the IGD directly. This remains a topic of future research, but we believe that the appropriate Bayes approach may offer a practical solution. As with the wTND, Bayes inference for the IGD is suggested purely on pragmatic (e.g., computational) reasons, but more analytical work is required to develop effective non-informative priors with this model. In general, however, we expect the basic

prescription of "product of uniform prior on $\mathbf{S}$ and Jeffreys prior on κ" plus "MHG sampling to approximate posteriors" to be reasonable for essentially any one-sample UARS model, including all those mentioned in this article. We note in closing that, treated as building blocks for more complicated models, UARS families including the wTND here and generalizations of the one-sample Bayes analyses have their place in regression, time series, spatial, and other kinds of statistical modeling and inference, such as two-level random effects problems with orientation data in materials science considered by Bingham et al. (2010).

Appendix

This note contains of the proofs of Propositions and the conventions of UARS densities.

A. Justification of Proposition 1

Here we use distributional properties of UARS-rotations, along with verifying general CLT conditions for rotations established by Parthasarathy (1964) and re-iterated by Nikolayev & Savyolova (1997). Without loss of generality, suppose $\mathbf{S} = \mathbf{I}_3$. From the UARS construction (1), the expectation $E(\mathbf{O}_{i,n}) = a_n \mathbf{I}_3$ follows, where $a_n = \frac{1}{3} + \frac{2}{3} E[\cos(r_{i,n}/\sqrt{n})]$. By Taylor expansion, $E[\cos(r_{i,n}/\sqrt{n})] = 1 - \frac{\sigma^2}{2n} + e_n$, where $|e_n| \leq \pi^3/n^{3/2}$. It then holds that

$$\overline{\lim}_{n\to\infty} n\{1 - \det[E(\mathbf{O}_{i,n})]\} = \overline{\lim}_{n\to\infty} n \left[1 - \left(1 - \frac{\sigma^2}{3n} + e_n\right)^3\right]$$

is bounded (equaling $\sigma^2 < \infty$) and that

$$\lim_{n\to\infty} n\,[\mathbf{I}_3 - E(\mathbf{O}_{i,n})] = \frac{\sigma^2}{3}\mathbf{I}_3.$$

By applying a result of Nikolayev & Savyolova (1997, Theorem 1), the proposition then follows where the concentration parameter in the isotropic Gaussian distribution on $SO(3)$ (see Table 1) is determined by $\kappa_{IG} = \sqrt{3}/\sigma$ (i.e, determined by the limiting scaled difference between the identity matrix and the mean $E(\mathbf{O}_{i,n})$ of a UARS rotation used in the composition). □

B Distribution of products of independent UARS-rotations

The following result shows that the UARS class of random rotations is closed under convolution.

Proposition 2 *Suppose* $\mathbf{O}_1, \ldots, \mathbf{O}_n$ *are independent (not necessarily identically distributed) random rotation matrices, each having some rotational distribution in the UARS class with mean rotation* $\mathbf{I}_3$*. Then, the rotational distribution of the product* $\mathbf{O}_1 \cdots \mathbf{O}_n$ *also belongs to the UARS class with mean rotation* $\mathbf{I}_3$*.*

To show the result, we use an alternative, but equivalent, definition of a UARS rotation. That is, if $|r|$ is randomly generated on $[0, \pi]$ and, conditional on $|r| \neq 0$, $\mathbf{u}\big||r|$ has a uniform distribution on the unit sphere in $\mathbb{R}^3$, then $\mathbf{O} = \mathbf{M}(|r|, \mathbf{u})$ from (1) belongs to the UARS class by definition with location $\mathbf{I}_3$. Using this, it suffices to consider $n = 2$ and Lemma 1 below to prove the proposition. That is, let $\mathbf{O}_1 = \mathbf{M}(|r_1|, \mathbf{u}_1)$ and $\mathbf{O}_2 = \mathbf{M}(|r_2|, \mathbf{u}_2)$ be independent rotations defined by independent $|r_1|, |r_2|$ where the conditional distribution $\mathbf{u}_i\big||r_i|$ is uniform on the unit sphere for $|r_i| \neq 0$, $i = 1, 2$. Let $\mathbf{H}$ be uniformly distributed on $SO(3)$ (cf. Miles, 1965) and independent of $\mathbf{O}_1$ and $\mathbf{O}_2$. Then, $|r_i| = \arccos[2^{-1}(tr(\mathbf{O}_i) - 1)]$ is independent of $\mathbf{H}$ and $\mathbf{H}\mathbf{u}_i\big||r_i| \stackrel{d}{=} \mathbf{u}_i\big||r_i|$ is uniform on the sphere for $|r_i| \neq 0$, $i = 1, 2$. We then have

$$\begin{aligned} \mathbf{H}^T\mathbf{O}_1\mathbf{O}_2\mathbf{H} = \mathbf{H}^T\mathbf{O}_1\mathbf{H}\mathbf{H}^T\mathbf{O}_2\mathbf{H} &= \mathbf{M}(|r_1|, \mathbf{H}\mathbf{u}_1)\mathbf{M}(|r_2|, \mathbf{H}\mathbf{u}_2) \\ &\stackrel{d}{=} \mathbf{O}(|r_1|, \mathbf{u}_1)\mathbf{O}(|r_2|, \mathbf{u}_2) = \mathbf{O}_1\mathbf{O}_2 \end{aligned}$$

and $\mathbf{O}_1\mathbf{O}_2$ belongs to the UARS class with mean rotation $\mathbf{I}_3$ by Lemma 1 below.

Lemma 1 *Let* $\mathbf{O} \in SO(3)$ *be a random rotation and* $\mathbf{H} \in SO(3)$ *be uniformly distributed and independent of* $\mathbf{O}$*. Then the distribution of* $\mathbf{O}$ *belongs to the UARS class with central direction* $\mathbf{I}_3$ *if and only if* $\mathbf{O} \stackrel{d}{=} \mathbf{H}^T\mathbf{O}\mathbf{H}$*.*

To justify Lemma 1, note that if $\mathbf{O} = \mathbf{M}(|r|, \mathbf{u})$, then $\mathbf{H}^T\mathbf{O}\mathbf{H} = \mathbf{M}(|r|, \mathbf{H}\mathbf{u})$. For all positive r, $\mathbf{H}\mathbf{u}\big||r|$ is uniform on the sphere (since $\mathbf{H}$ is uniform on $SO(3)$). The distributions of $\mathbf{O}$ and $\mathbf{H}^T\mathbf{O}\mathbf{H}$ are equal if and only if those of $\mathbf{H}\mathbf{u}\big||r|$ and $\mathbf{u}\big||r|$ are equal for $|r| \neq 0$, which occurs if and only if $\mathbf{O}$ belongs to the UARS class.

C Domain-specific conventions for expressing UARS-rotation densities

Suppose $\mathbf{O} = \mathbf{M}(r, \mathbf{u})$ denotes a random rotation resulting from the UARS construction (1) with location parameter $\mathbf{S} = \mathbf{I}_3$ and a random spin r based on an angular density $g(r|\kappa)$, $r \in (-\pi, \pi]$ (with respect to the Lesbesgue measure), symmetric around zero with concentration parameter $\kappa > 0$. From Section 2.1, recall that rotation $\mathbf{O}$ has a density with respect to the uniform distribution on $SO(3)$ given by

$$f(\mathbf{O}|\kappa) = \frac{4\pi}{3 - tr(\mathbf{O})} g(\arccos[2^{-1}(tr(\mathbf{O}) - 1)]|\kappa), \quad \mathbf{O} \in SO(3). \tag{6}$$

From (1), we have the relationships $tr(\mathbf{O}) = 1 + 2\cos(r)$ and $|r| = \arccos[2^{-1}(tr(\mathbf{O}) - 1)]$ which then can be used to go back and forth, equivalently, between $f(\mathbf{O}|\kappa)$ and $g(r|\kappa)$.

In this paper, we represent rotational distributions from the UARS class in terms of their angular densities $g(r|\kappa)$, $r \in (-\pi, \pi]$ (see, for example, Table 1). However, in the material science literature, it is common (cf. Matthies et al., 1988; Nikolayev & Savyolova, 1997) to display probability densities graphically as

$$h(r|\kappa) = \frac{2\pi}{1 - \cos r} g(r|\kappa), \quad r \in (0, \pi], \tag{7}$$

which expresses the *rotational* density (6) as a function of the Euler angle r. In the texture analysis literature, $|r|$ is often referred to as a misorientation angle in the Euler axis-angle representation of a rotation $\mathbf{O} = \mathbf{M}(r, \mathbf{u}) = \mathbf{M}(|r|, \text{sign}(r)\mathbf{u})$ (see Section 6). Note that $|r|$ has density $2g(r|\kappa)$ on $(0, \pi]$ while the misorientation angle from the uniform distribution on $SO(3)$ has density $(1 - \cos r)/\pi$, $r \in (0, \pi]$. That is, (7) is a ratio for comparing misorientation angles densities from a UARS model to the uniform model on $SO(3)$. However, the function in (7) is *not* a probability density on $(0, \pi]$ and, to avoid confusion, we have elected to frame our exposition in terms of Euler angle densities on $(-\pi, \pi]$.

Bibliography

[1] Bingham, M.A., Lograsso, B.K. and Laabs, F.C. (2010). A Statistical Analysis of the Variation in Measured Crystal Orientations Obtained Through Electron Backscatter Diffraction. *Journal of Ultramicroscopy* **110**, 1312-1319.

[2] Bingham, M.A., Nordman D.J. and Vardeman, S.B. (2009a). Modeling and Inference for Measured Crystal Orientations and a Tractable Class of Symmetric Distributions for Rotations in Three Dimensions. *Journal of the American Statistical Association* **104**, 1385-1397.

[3] Bingham, M.A., Vardeman, S.B. and Nordman D.J. (2009b). Bayes One-Sample and One-Way Random Effects Analyses for 3-D Orientations with Application to Materials Science. *Bayesian Analysis* **4**, 607-630.

[4] Bingham, M.A., Nordman D.J. and Vardeman, S.B. (2009c). Finite-Sample Investigation of Likelihood and Bayes Inference for the Symmetric von Mises-Fisher Distribution. *Computational Satatistics and Data Analysis* **54**, 1317-1327.

[5] Borovkov, M. and Savyolova, T. (2007). The Computational Approaches to Calculate Normal Distributions on the Rotation Group. *Journal of Applied Crystallography* **40**, 449-455.

[6] Bucharova, T.I. and Savyolova, T.I. (1993). Application of Normal Distributions on SO(3) and S^n for Orientation Distribution Function Approximation. *Textures and Microstructures* **21**, 161-176.

[7] Bunge, H.J. (1982). *Texture Analysis in Material Science*. Butterworth, London.

[8] Chang, T. (1998). Estimating the Relative Rotation of Two Tectonic Plates from Boundary Crossings. *Journal of the American Statistical Association* **83**, 1178-1183.

[9] Chang, T. and Rivest, L.-P. (2001). M-Estimation for Location and Regression Parameters in Group Models: A Case Study Using Stiefel Manifolds. *The Annals of Statistics* **29**, 784-814.

[10] Chirikjian, G.S. (2009). *Stochastic Models,Information Theory,and Lie Groups.* Birkhäuser, Boston.

[11] Downs, T.D. (1972). Orientation Statistics. *Biometrika* **59**, 665-676.

[12] Peckham, G.D. and McNaught, I.J. (1992). Applications of the Maxwell-Boltzmann Distribution. *Journal of Chemical Education* **69**, 554-558.

[13] Hartman, P. and Watson, G. S. (1974). Normal Distribution Functions on Spheres and the Modified Bessel Functions. *The Annals of Probability* **2**, 593-607.

[14] Hielscher, R. (2010). Kernel density estimation on the rotation group. Preprint 2010-7, Fakultät für Mathematik, TU Chemnitz.

[15] Hielscher, R., Schaeben, H. and Siemes H. (2010). Orientation Distribution Within a Single Hematite Crystal. *Mathematical Geosciences* **42**, 359-375.

[16] Jupp, P.E. and Mardia, K.V. (1979). Maximum likelihood estimators for the Matrix Von Mises-Fisher and Bingham distributions. *Ann. Statist.* **7**, 599-606.

[17] Jupp, P.E. and Mardia, K.V. (1989). A Unified View of the Theory of Directional Statistics, 1975-1988. *International Statistical Review* **57**, 261-294.

[18] Kent, J. (1978). Limiting Behaviour of the von Mises-Fisher Distribution. *Mathematical Proceedings of the Cambridge Philosophical Society* **84**, 531-536.

[19] Khatri, C.G. and Mardia, K.V. (1977). The Von Mises-Fisher Matrix distribution in orientation statistics. *J. Roy. Statist. Soc. Ser. B*, **39**, 95-106.

[20] León, C.A., Massé, J.-C. and Rivest L.-P. (2006). A Statistical Model for Random Rotations. *Journal of Multivariate Analysis* **97**, 412-430.

[21] Mardia, K.V. (1975). Statistics of Directional Data. *Journal of the Royal Statistical Society, Series B* **37**, 349-393.

[22] Mardia, K.V. and Jupp, P.E. (2000). *Directional Statistics*. Wiley, New York.

[23] Matthies, S. (1982). Form Effects in the Description of the Orientation Distribution Function (ODF) of Texturized Materials by Model Components. *Physica Status Solidi (b)* **112**, 705-716.

[24] Matthies, S., Muller,J. and Vinel, G.W. (1988). On the Normal Distribution in the Orientation Space. *Textures and Microstructures* **10**, 77-96.

[25] Miles, R.E. (1965). On Random Rotations in $\mathbb{R}^3$. *Biometrika* **52**, 636-639.

[26] Nikolayev D.I. and Savyolova, T.I. (1997). Normal Distribution on the Rotation Group $SO(3)$. *Textures and Microstructures* **29**, 201-233.

[27] Nordman, D.J. Vardeman, S.B. and Bingham, M.A. (2009). Uniformly Hyper-efficient Bayes Inference in a Class of Non-regular Problems. *The American Statistician* **63**, 234-238.

[28] Parthasarathy, K.P. (1964). The Central Limit Theorem for the Rotation Group. *Theory of Probability and its Applications* **9**, 273-282.

[29] Prentice,M.J. (1986). Orientation statistics without parametric assumptions. *Journal of Royal Statistics Society: Series B* **48**, 214-222.

[30] Randle, V. (2003). *Microtexture Determination and its Applications*, London: Maney for The Institute of Materials, Minerals and Mining.

[31] Rancourt, D., Rivest, L. P. and Asselin, J. (2000). Using orientation statistics to investigate variations in human kinematics. *J. Roy. Statist. Soc. Ser. C* **49**, 81-94.

[32] Roberts, P.H. and Ursell, H.D. (1960). Random Walk on a Sphere and on a Riemannian Manifold. *Philosophical Transactions of the Royal Society of London Series A* **252**, 317-356.

[33] Savyolova, T.I. (1984). Distribution Functions of Grains with Respect to Polycrystal Orientations and Its Gaussian Approximations. *Industrial Laboratory* **50**, 468-474.

[34] Schaeben, H. (1992). "Normal" orientation distributions. *Textures and Microstructures* **19**, 197-202.

[35] Schaeben, H. (1997). The de la Vallée Poussin Standard Orientation Density Function *Textures and Microstructures* **33**, 365-373.

[36] Schaeben, H. and Nikolayev, D.I. (1998). The Central Limit Theorem in Texture Component Fit Methods. *Acta Applicandae Mathematicae* **53**, 59-87.

[37] Stavdahl, O., Bondhus, A.K., Pettersen, K.Y. and Malvig, K.E. (2005). Optimal statistical operators for 3-dimensional rotational data: geometric interpretations and application to prosthesis kinematics. *Robotica* **3**, 283-292.

[38] Watson, G. S. (1983). *Statistics on Spheres*. Wiley, New York.

CHAPTER 3. ONE-SAMPLE BAYES INFERENCE FOR SYMMETRIC DISTRIBUTIONS OF 3-D ROTATIONS

A paper Modified from a paper to be published in *The Journal of Computational Statistics and Data Analysis*

Yu Qiu, Daniel J. Nordman and Stephen B. Vardeman

Abstract

A variety of existing symmetric parametric models for 3-D rotations found in both statistical and materials science literatures are considered from the point of view of the "uniform-axis-random-spin" (UARS) construction. One-sample Bayes methods for non-informative priors are provided for all of these models and attractive frequentist properties for corresponding Bayes inference on the model parameters are confirmed. Taken together with earlier work, the broad efficacy of non-informative Bayes inference for symmetric distributions on 3-D rotations is conclusively demonstrated.

1 Introduction

This paper concerns statistical analysis for orientations in three dimensions as represented by 3×3 rotation matrices. Probability models for 3-D orientations are used in many application areas including crystallography and quantitative texture analysis in materials science. There, variation in orientation of crystal structures across a specimen is related to macro-level physical properties of a material. Symmetric or isotropic (i.e., having central or rotationally invariant densities about a central rotation) distributions have been of most interest in materials applications.

Bingham et al. (2009a) studied the "uniform-axis-random-spin" (UARS) class of 3-D rotations using Euler's angle-axis representation. The construction used there is as follows. Let $\mathbf{u} = (u_1, u_2, u_3)^T$ be uniformly distributed over the $\mathbb{R}^3$ unit sphere S^2 and, independently, r be a random angle on $(-\pi, \pi]$ drawn from a symmetric density $C(\cdot|\kappa)$ whose spread is controlled by a concentration parameter $\kappa > 0$. Then a random UARS rotation with mean direction $\mathbf{I}_3$ is given by

$$\mathbf{M}(r, \mathbf{u}) = (\cos r)\mathbf{I}_3 + (\sin r)\mathbf{A}(\mathbf{u}) + (1 - \cos r)\mathbf{u}\mathbf{u}^T, \tag{1}$$

which is a rotation by a random angle r about the random vector $\mathbf{u}$. Subsequently, a UARS observation with mean rotation $\mathbf{S}$ (a fixed parameter) $\in SO(3)$ (the set of 3×3 orthogonal matrices with determinant 1) is defined as $\mathbf{O} = \mathbf{S} \cdot \mathbf{M}(r, \mathbf{u})$ (or equivalently $\mathbf{M}(r, \mathbf{u}) \cdot \mathbf{S}$), representing a directionally symmetric perturbation of $\mathbf{S}$. The construction is simple and physically motivated and the interpretation is intuitive, see Leòn et al. (2006, sec. 5.2) and Qiu et al. (2013). UARS distributions appearing in the statistical and materials science literatures include the von-Mises (vM) UARS distribution (Bingham et al., 2009b), the isotropic Matrix Fisher distribution (Downs, 1972), the Lorentzian distribution (Matthies, 1982), Bunge's Gaussian distribution (Bunge, 1982), the isotropic Gaussian distribution (Borovkov & Savyolova, 2007; Matthies et al., 1988; Nikolayev & Savyolova, 1997; Savyolova, 1985; Schaeben, 1992;), the de la Vallèe Poussin distribution (Schaeben, 1997)(i.e., the Cayley distribution (Leòn et al., 2006)), and the wrapped trivariate normal (wTN) UARS distribution (Qiu et al., 2013). All these distributions have the UARS structure with different choices of angular distributions.

Most existing works for distributions on rotations focus on likelihood-based inference and moment estimation (see for example Chang and Rivest, 2001; Jupp and Mardia, 1979; Leòn et al., 2006; Oualkacha and Rivest, 2008) and consider large sample properties. Large-sample estimation results typically fail to provide easily interpretable (in terms of their geometry) confidence regions for the parameter $\mathbf{S}$, and therefore do not clearly convey information about statistical precision. In contrast, the Bayes methods presented in this paper provide credible regions for $\mathbf{S}$ which have not only a simple geometrical structure indicating precision, but also frequentist coverage properties matching the credible levels.

In this paper we explore one-sample Bayes inference for the two parameters of all UARS distributions that have appeared in the literature plus that for a new wrapped normal (wN) UARS distribution. In Section 2, we first review the forms of all published UARS distributions and identify non-informative priors for the mean rotation and concentration parameters. In Section 3, we identify the corresponding posterior distributions and summarize a general MCMC construction of cone-based confidence regions for mean rotation parameters. In Section 4, a simulation study for one-sample Bayes inferences is provided in order to establish the frequentist properties for the Bayes methods in all UARS models. Section 5 summarizes and suggests future work. An online Supplementary Appendix provides the details of calculations of Fisher information functions for all angular distributions (distributions of r) employed here.

2 Models and Priors for the Parameters

Before listing the models in the UARS class that have been studied in the literature, it is worthwhile to reiterate the general expression for an orientation density function (ODF), which is a probability density function on $SO(3)$ in the UARS class. Given an angular density $C(r|\kappa)$, defined on $(-\pi, \pi]$ and symmetric about zero with concentration parameter κ, and a fixed mean rotation parameter $\mathbf{S} \in SO(3)$, a UARS observation $\mathbf{O}$ has a density with respect to the uniform distribution on $SO(3)$ of the form

$$f(\mathbf{O}|\mathbf{S}, \kappa) = \frac{4\pi}{3 - tr(\mathbf{S}^T\mathbf{O})} C(\arccos[2^{-1}(tr(\mathbf{S}^T\mathbf{O}) - 1)]|\kappa), \mathbf{O} \in SO(3) \tag{2}$$

where $tr(\cdot)$ and $(\cdot)^T$ denote respectively the matrix trace and transpose; see Bingham et al. (2009a) for details.

For Bayes inference, we must identify appropriate priors for the model parameters. Following the approach of Bingham et al. (2009b), we use the uniform distribution on $SO(3)$ (which has the ODF $p(\mathbf{O}) = 1$ corresponding to an angular density $C(r) = [1 - \cos(r)]/(2\pi)$ in (1) for $r \in (-\pi, \pi]$) as the prior for the location parameter $\mathbf{S}$, and adopt (an independent) Jeffreys prior for the concentration parameter, κ.

To be consistent with the discussion in Qiu et al. (2013), we consider the corresponding Jeffreys prior for the spread parameter $\eta = -\log\kappa$ which has density

$$J(\eta) = \exp(-\eta)\sqrt{\mathcal{I}(\exp(-\eta))}, \quad \eta \in (-\infty, \infty) \tag{3}$$

with Fisher information function corresponding to the angular density $C(r|\kappa)$

$$\mathcal{I}(\kappa) = -E\left[\frac{d^2}{d\kappa^2}\log(C(r|\kappa))\right] \quad \kappa > 0.$$

Details of the derivations of $\mathcal{I}(\kappa)$ for the various cases considered in this paper are collected in the online Appendix.

Each ODF in the UARS class is completely determined by the angular density $C(r|\kappa)$. If $\lim_{r\to 0}\frac{C(r|\kappa)}{1-\cos r}$ is not finite, the ODF (1) is unbounded at $\mathbf{O} = \mathbf{S}$ and the corresponding model is non-regular. Estimators of the parameter $\mathbf{S}$ exhibit different asymptotic (as the sample size $n \to \infty$) behavior in non-regular models than in regular cases. So based on the forms of the angular densities $C(r|\kappa)$, we organize our presentation of the UARS models by first considering regular cases (IG, Bunge's Gaussian, isotropic Matrix Fisher, de la Vallée Poussin (i.e. isotropic Cayley), and Lorentzian UARS distributions), and then non-regular cases (von-Mises, wTN, and wN UARS distributions).

2.1 Regular Cases

For these distributions, $\lim_{r\to 0}\frac{C(r|\kappa)}{1-\cos r}$ is finite. We use the same notation, κ, for the concentration parameters for all regular distributions. Except for the Lorentzian case, these distributions become essentially identical (all approximating the isotropic Gaussian distribution) for large κ.

2.1.1 Isotropic Gaussian Angular Distribution

The density for the isotropic Gaussian angular distribution is

$$C_{IG}(r|\kappa) = \frac{1-\cos r}{2\pi} \sum_{m=0}^{\infty} (2m+1) \exp\left[-m(m+1)/(2\kappa^2)\right] \frac{\sin\left[(m+1/2)r\right]}{\sin(r/2)},$$

$r \in (-\pi, \pi]$ (Matthies et al., 1988; Savyolova, 1985). The corresponding Fisher information function is

$$\begin{aligned} \mathcal{I}(\kappa) &= \frac{1}{\kappa^6} \int_{-\pi}^{\pi} \frac{1-\cos r}{2\pi} \frac{\left[\sum_{m=0}^{\infty} m(m+1) f(r|m,\kappa)\right]^2}{\sum_{m=0}^{\infty} f(r|m,\kappa)} dr \\ &\quad - \frac{1}{\kappa^6} \int_{-\pi}^{\pi} \frac{1-\cos r}{2\pi} \sum_{m=0}^{\infty} \left[m^2(m+1)^2 - 3m(m+1)\kappa^2\right] f(r|m,\kappa) dr, \end{aligned}$$

where $f(r|m,\kappa) = (2m+1)\exp\left[-m(m+1)/(2\kappa^2)\right] \frac{\sin[(m+0.5)r]}{\sin(r/2)}$.

As $\eta \to \infty, J(\eta) \to 0$ and as $\eta \to -\infty, J(\eta) \to \sqrt{6}$. The Jeffreys prior does not have a simple closed form, but can be computed numerically. We use $J(\eta) \approx \sqrt{6}$ when $\eta < -2$, $J(\eta) \approx 0$ when $\eta > 2$ and, for $-2 \le \eta \le 2$, we fit a cubic spline to approximate $J(\eta)$ after calculating the density at grid points $-2 + 0.004i, i = 0, 1, \ldots, 1000$.

2.1.2 Bunge Angular Distribution

The density for the Bunge angular distribution is

$$C_{Bunge}(r|\kappa) = \frac{1-\cos r}{2\pi} N(\kappa) \exp\left[-\kappa^2 r^2/2\right], \quad r \in (-\pi, \pi]$$

with a normalizing constant $N(\kappa)$ (Bunge, 1982). The corresponding Fisher information function is

$$\mathcal{I}(\kappa) = E(r^2) - \frac{d^2 \log(N(\kappa))}{d\kappa^2}.$$

As $\eta \to \infty, J(\eta) \to 0$, and as $\eta \to -\infty, J(\eta) \to \sqrt{6}$. We use $J(\eta) \approx \sqrt{6}$ when $\eta < -2, J(\eta) \approx 0$ when $\eta > 3$ and, for $-2 \le \eta \le 3$, we fit a cubic spline to approximate $J(\eta)$ after

calculating the Jeffreys density at grid points $-2 + 0.005i, i = 0, 1, \ldots, 1000$.

2.1.3 de la Vallée Poussin Angular Distribution

The density for the de la Vallée Poussin angular distribution is

$$C_{Poussin}(r|\kappa) = \frac{1 - \cos r}{2\pi} \frac{B(3/2, 1/2)}{B(3/2, 2\kappa^2 + 1/2)} \cos^{4\kappa^2}(r/2),\ r \in (-\pi, \pi]$$

(Schaeben, 1997). León et al. (2006) later derived the same distribution, calling it the Cayley distribution and providing an equivalent form for the density

$$C_{Cayley}(r|\kappa) = \frac{1 - \cos r}{2\pi} \frac{\sqrt{\pi}\Gamma(2\kappa^2 + 2)(1 + \cos r)^{2\kappa^2}}{2^{2\kappa^2}\Gamma(2\kappa^2 + 1/2)}, \quad r \in (-\pi, \pi].$$

The corresponding Fisher information function is

$$\begin{aligned} \mathcal{I}(\kappa) &= 4\left[\psi_0(2\kappa^2 + 1/2) - \psi_0(2\kappa^2 + 2)\right] + 16\kappa^2\left[\psi_1(2\kappa^2 + 1/2) - \psi_1(2\kappa^2 + 2)\right] \\ &\quad -8E\left\{\log\left[\cos(r/2)\right]\right\} \end{aligned}$$

where ψ_n is the polygamma function.

As $\eta \to \infty, J(\eta) \to 0$, and as $\eta \to -\infty, J(\eta) \to \sqrt{6}$. We use $J(\eta) \approx \sqrt{6}$ when $\eta < -2, J(\eta) \approx 0$ when $\eta > 4$ and, for $-2 \leq \eta \leq 4$, we fit a cubic spline to approximate $J(\eta)$ after calculating the density at grid points $-2 + 0.006i, i = 0, 1, \ldots, 1000$.

2.1.4 Lorentzian Angular Distribution

The density for the Lorentzian angular distribution is

$$C_{Lorentzian}(r|\kappa) = \frac{1 - \cos r}{2\pi}(1 + \lambda)\frac{(1 + 2\lambda)^2 + 4\lambda(\lambda + 1)\cos^2(r/2)}{\left[(1 + 2\lambda)^2 - 4\lambda(\lambda + 1)\cos^2(r/2)\right]^2},\ r \in (-\pi, pi]$$

(Matthies, 1982). Letting $\lambda = \kappa/2 - 0.5 + 2/(\kappa + 2)^2$ puts the Lorentzian distribution on roughly the same scale as the others, but for large κ, the Lorentzian shape differs from that of

the other distributions considered here. The corresponding Fisher information function is

$$\begin{aligned}\mathcal{I}(\kappa) &= \frac{12}{(\kappa+2)^4}\int_{-\pi}^{\pi} C'(r|\lambda)dr + \left[1/2 - 4/(\kappa+2)^3\right]^2 \int_{-\pi}^{\pi} C''(r|\lambda)dr \\ &\quad - \left[1/2 - 4/(\kappa+2)^3\right]^2 \int_{-\pi}^{\pi} \frac{\left[C'(r|\lambda)\right]^2}{C(r|\lambda)}dr.\end{aligned}$$

As $\eta \to \infty, J(\eta) \to 0$, and as $\eta \to -\infty, J(\eta) \to 1$. We use $J(\eta) \approx 1$ when $\eta < -2, J(\eta) \approx 0$ when $\eta > 8$ and, for $-2 \leq \eta \leq 8$, we fit a cubic spline to approximate $J(\eta)$ after calculating the density at grid points $-2 + 0.01i, i = 0, 1, \ldots, 1000$.

2.1.5 Isotropic Matrix Fisher Angular Distribution

Bingham et al. (2010a) have treated the isotropic Matrix Fisher (MF) UARS distribution. Here, to be consistent with the parameterizations of the other regular distributions for large κ, we parameterize its angular density as

$$C_{MF}(r|\kappa) = \frac{1-\cos r}{2\pi}\frac{\exp(k^2\cos r)}{I_0(k^2) - I_1(k^2)}, \quad r \in (-\pi, \pi]$$

where I_i denotes the modified Bessel function of order i. The corresponding Fisher information function is

$$\mathcal{I}(\kappa) = -2E\left(\cos r\right) - 2 + \frac{2I_1^2(\kappa^2) - 6I_1(\kappa^2)I_0(\kappa^2)}{\kappa^2\left[I_0(\kappa^2) - I_1(\kappa^2)\right]^2} + \frac{4\left[I_0(\kappa^2) + I_1(\kappa^2)\right]}{I_0(\kappa^2) - I_1(\kappa^2)}.$$

As $\eta \to \infty, J(\eta) \to 0$, and as $\eta \to -\infty, J(\eta) \to \sqrt{6}$.

2.2 Non-regular Cases

For these angular distributions, $\lim_{r\to 0} \frac{C(r|\kappa)}{1-\cos r}$ is infinite and the UARS ODF (1) has a singularity at $\mathbf{O} = \mathbf{S}$.

2.2.1 Wrapped Normal Angular Distribution

Unlike the angular densities for regular UARS models, the wN angular density is unimodal on $(-\pi, \pi]$ with expression

$$C_{wN}(r|\kappa) = \frac{1}{\kappa^2} + \frac{\kappa}{\sqrt{2\pi}} \int_{-\pi}^{\pi} \sum_{m=-\infty}^{\infty} (2m\pi - r)^2 g(r|m, \kappa) dr, \quad r \in (-\pi, \pi].$$

The corresponding Fisher information function is

$$\begin{aligned} \mathcal{I}(\kappa) &= \frac{1}{\kappa^2} + \frac{\kappa}{\sqrt{2\pi}} \int_{-\pi}^{\pi} \sum_{m=-\infty}^{\infty} (2m\pi - r)^2 g(r|m, \kappa) dr \\ &\quad + \frac{\kappa^3}{\sqrt{2\pi}} \int_{-\pi}^{\pi} \sum_{-\infty}^{\infty} (2m\pi - r)^4 g(r|m, \kappa) dr - \frac{\kappa^3}{\sqrt{2\pi}} \int_{-\pi}^{\pi} \frac{\left[\sum_{-\infty}^{\infty} (2m\pi - r)^2 g(r|m, \kappa)\right]^2}{\sum_{-\infty}^{\infty} g(r|m, \kappa)} dr, \end{aligned}$$

where $g(r|m, \kappa) = \exp\left(-(2m\pi - r)^2 \kappa^2 / 2\right)$.

As $\eta \to \infty, J(\eta) \to 0$, and as $\eta \to -\infty, J(\eta) \to \sqrt{2}$. We use $J(\eta) \approx 1$ when $\eta < -0.5, J(\eta) \approx 0$ when $\eta > 2$ and, for $-0.5 \leq \eta \leq 2$, we fit a cubic spline to approximate $J(\eta)$ after calculating the density at grid points $-0.5 + 0.0025i, i = 0, 1, \ldots, 1000$.

2.2.2 Von-Mises Angular Distribution

Bingham et al. (2009b) have used the von-Mises (vM) angular distribution for modeling rotations in texture analysis. For consistency with the wrapped normal angular density, we parameterize this density as

$$C_{vM}(r|\kappa) = \frac{\exp(\kappa^2 \cos r)}{2\pi I_0(\kappa^2)}, \quad r \in (-\pi, \pi].$$

where I_i denotes the modified Bessel function of order i. And the corresponding Fisher information function is

$$\mathcal{I}(\kappa) = -2E\left(\cos r\right) - 4\kappa^2 \frac{I_1^2(\kappa^2)}{I_0^2(\kappa^2)} - \frac{2I_1(\kappa^2)}{I_0(\kappa^2)} + 4\kappa^2.$$

As $\eta \to \infty, J(\eta) \to 0$, and as $\eta \to -\infty, J(\eta) \to \sqrt{2}$.

2.2.3 Wrapped Trivariate Normal Model

Qiu et al. (2013) have introduced the wrapped trivariate normal (wTN) model for random rotations, and it is worthwhile to reiterate the form of its angular distribution. This is

$$C_{wTN}(r|\kappa) = \sum_{m=-\infty}^{\infty} \frac{\kappa^3}{\sqrt{2\pi}}(2m\pi - r)^2 \exp\left[-\kappa^2(2m\pi - r)^2/2\right], \quad r \in (-\pi, \pi].$$

and the corresponding Fisher information function is

$$\mathcal{I}(\kappa) = -\frac{9}{\kappa^2} + \frac{\kappa^5}{\sqrt{2\pi}} \int_{-\pi}^{\pi} \frac{\left\{\sum_{m=-\infty}^{\infty} (2m\pi - r)^4 \exp\left[-\kappa^2(2m\pi - r)^2/2\right]\right\}^2}{\sum_{m=-\infty}^{\infty} (2m\pi - r)^2 \exp\left[-\kappa^2(2m\pi - r)^2/2\right]} dr.$$

As $\eta \to \infty, J(\eta) \to 0$, and as $\eta \to -\infty, J(\eta) \to \sqrt{6}$.

2.3 Visual Summary of Models and Jeffreys Priors

For visual comparison purposes, plots of 8 sets of angular densities and the corresponding Jeffreys prior densities (here we rescale the Jeffreys prior densities such that they converge to 1 as η goes to $-\infty$) are given in Figures 1 and 2.

3 One-Sample Bayes Inference

We consider one-sample Bayes inference using the improper Jeffreys priors for concentration parameters and uniform distributions for central orientation parameters. For n observations $\mathbf{O}_i, i = 1, \ldots, n$ from some UARS density (1), the corresponding likelihood function is

$$L(\mathbf{O}_1, \ldots, \mathbf{O}_n|\mathbf{S}, \eta) \propto \frac{\prod_{i=1}^{n} C\left(\arccos\left[2^{-1}(tr(\mathbf{S}^T\mathbf{O}_i) - 1)\right] | \exp(-\eta)\right)}{\prod_{i=1}^{n} [3 - tr(\mathbf{S}^T\mathbf{O}_i)]}.$$

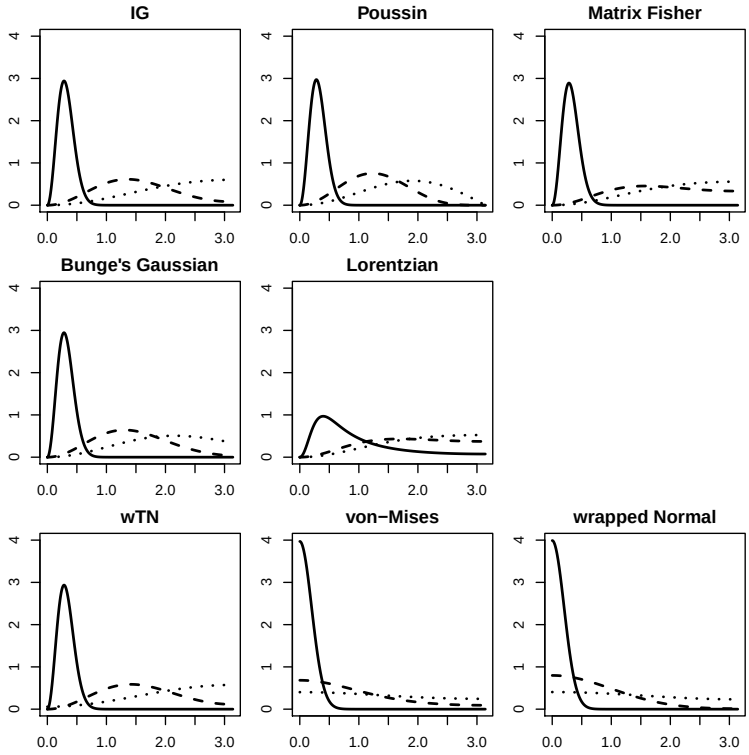

Figure 1 Absolute angular densities (i.e., densities for $|r|$) when κ =0.5(dotted), 1(dashed), 5(solid).

Multiplying by prior densities $p(\mathbf{S})$ and $J(\eta)$ gives a posterior density $h(\mathbf{S}, \eta)$ for $(\mathbf{S}, \eta)$ proportional to

$$\frac{\prod_{i=1}^{n} C\left(\arccos\left[2^{-1}(tr(\mathbf{S}^T\mathbf{O}_i) - 1)\right] | \exp(-\eta)\right)}{\prod_{i=1}^{n} [3 - tr(\mathbf{S}^T\mathbf{O}_i)]} J(\eta).$$

We may sample a sequence of pairs, $(\mathbf{S}_j, \eta_j)$, from the posterior distribution using the basic Metropolis-Hastings-within-Gibbs (MHG) algorithm of Bingham et al. (2009bc) as follows. With observations $\mathbf{O}_1, \ldots, \mathbf{O}_n \in SO(3)$ and the starting values $\mathbf{S}_0, \eta_0$:

- Generate $\mathbf{S}^{j^*}$ from the isotropic Matrix Fisher rotational distribution with location parameter $\mathbf{S}^{j-1}$ and concentration parameter ρ. (Here ρ is a tuning parameter.)
- Compute $r_j^1 = \frac{h(\mathbf{S}^{j^*}, \eta^{j-1})}{h(\mathbf{S}^{j-1}, \eta^{j-1})}$ and generate $W_j^1 \sim$ Bernoulli$(\min(1, r_j^1))$. Take $\mathbf{S}^j = W_j^1 \mathbf{S}^{j^*} + (1 - W_j^1)\mathbf{S}^{j-1}$.
- Generate $\eta^{j^*} \sim N(\eta^{j-1}, \gamma^2)$. (Here γ is a tuning parameter.)

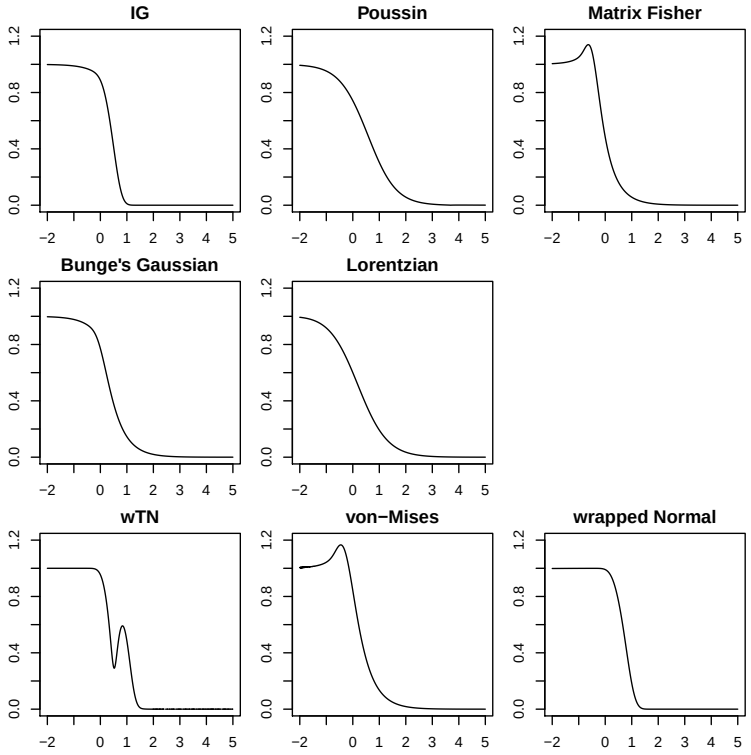

Figure 2 Rescaled Jeffreys prior densities of $\eta = -\log\kappa$ for all 8 angular distributions.

- Compute $r_j^2 = \frac{h(\mathbf{S}^j, \eta^{j^*})}{h(\mathbf{S}^j, \eta^{j-1})}$ and generate $W_j^2 \sim \text{Bernoulli}(\min(1, r_j^2))$. Take $\eta^j = W_j^2 \eta^{j^*} + (1 - W_j^2)\eta^{j-1}$.

With the simulated $\mathbf{S}$ and η, we can create approximately 95% credible regions for the parameters. One advantage of the Bayes method is that we can construct a geometrically interpretable credible region for the mean rotation $\mathbf{S}$ using the "sets of cones" idea in Bingham et al. (2009b) as follows. First, we define a Bayes point estimator $\mathbf{S}_B$ as the maximizer of $tr(\mathbf{S}_B^T \bar{\mathbf{S}})$ (i.e., the Bayes estimator under a squared error loss function $tr[(\mathbf{S}_B - \mathbf{S})(\mathbf{S}_B - \mathbf{S})^T]$), based on the average $\bar{\mathbf{S}}$ of $100,000$ orientations $\mathbf{S}_i, i = 1, ..., 100,000$ simulated from the posterior. Then we obtain a set of cones around positive parts of axes representing $\mathbf{S}_B$ with angle a as the boundary of a 95% credible region for $\mathbf{S}$ (where a is the 95th percentile of $a_1, ..., a_{100,000}$ and each a_j represents the maximum arccosine value (between 0 and π) of the diagonal elements of $\mathbf{S}_B^T \bar{\mathbf{S}}$). Details of the method and graphical interpretations can be found in Bingham et al. (2009bc), and Qiu et al. (2013). The value of the angle between the center and edge of the

cones can be used as a measure of size of the credible region for $\mathbf{S}$.

Even with small sample size, the UARS distributions are distinguishable from each other when κ is small. One can investigate which UARS distribution best describes an orientation data set by plotting the cumulative distribution function of the absolute misorientation angles with Bayes estimated parameter $\hat{\kappa}$ for each distribution against the empirical distribution of misorientation angles $\{\widehat{|r|}_i : i = 1, \ldots, n\}$, computed as $\widehat{|r|}_i = \arccos\{[tr(\hat{\mathbf{S}}^T \boldsymbol{O}_i) - 1]/2\}$ using a non-parametric "moment" estimator $\hat{\mathbf{S}}$ of the mean rotation for de-trending defined as the maximizer of $\sum_i tr(\boldsymbol{S}^T \boldsymbol{O}_i)$. See Qiu et al. (2013) for details. Bingham et al. (2009a) used this kind of plotting method with a small data set (of size $n = 14$) to demonstrate the effectiveness of the von-Mises UARS model in a materials science application where the existing regular models failed to provide adequate descriptions of the real data. Qiu et al. (2013) used this kind of plotting method with a data set of moderate size (of size $n = 112$) to demonstrate the effectiveness of the wTN UARS model compared to isotropic Gaussian and matrix Fisher UARS models.

In the next section, we describe a simulation study using the MCMC algorithm to perform one-sample Bayes analyses (for the UARS distributions with Bayes methods not yet treated in the literature) for several choices of η and n. We then summarize the frequentist coverage probabilities and sizes of credible regions obtained from the Bayes methods and thereby establish the effectiveness of the non-informative Bayes methods.

4 Simulation Results

To simulate test data sets from the UARS distributions, we chose the values of the parameter η to be $-1.844, -1.151, -0.347, 0, 0.5, 1$ and sample sizes $n = 10, 30, 100, 300, 1000$. We held the parameter $\mathbf{S}$ constant at $\mathbf{I}_3$ as the choice of $\mathbf{S}$ is irrelevant (Bingham et al. 2009a).

For each UARS distribution with one combination of sample size n and parameter η, we simulated $4,000$ data sets, each consisting of a random sample of n observations. For each data set, we generated $100,000$ samples from the posterior distribution using the MHG algorithm after a $25,000$ iteration burn-in period. (The starting values for $\mathbf{S}_0$ and η_0 in the simulation

study were chosen to be the true parameters, as we determined that the choice of starting values did not affect posterior simulation results with a $25,000$ iteration burn-in period.) The tuning parameters ρ and γ were chosen to keep the Metropolis-Hastings jumping rates between 30% and 40% and are given in Table 1.

Table 1 Values of tuning parameters ρ and γ for MCMC.

	IG		Bunge		de la Vallée Poussin		Lorentzian		wrapped Normal	
(n,η)	ρ	γ	ρ	γ	ρ	γ	ρ	γ	ρ	γ
(10,1)	0.02	0.65	1.9	0.5	7.75	0.5	0.14	0.9	34.64	0.4
(30,1)	16.12	0.65	20	0.5	20	0.5	4	0.5	77.46	0.25
(100,1)	200	0.65	63.25	0.5	40	0.25	1.55	0.3	244.94	0.12
(300,1)	316.22	0.65	126.49	0.5	100	0.2	13	0.2	774.6	0.05
(1000,1)	1000	0.65	860.23	0.5	24.26	0.15	18.97	0.12	2236.07	0.02
$(10, 0.5)$	4.47	0.65	0.45	0.5	0.04	0.5	0.14	0.9	40	0.4
$(30, 0.5)$	27.75	0.5	1.26	0.45	2	0.5	1.26	0.45	63.25	0.25
$(100, 0.5)$	83.67	0.5	2	0.3	2	0.35	1	0.3	200	0.12
$(300, 0.5)$	77.46	0.5	2.24	0.2	3.16	0.2	10.95	0.15	346.41	0.05
$(1000, 0.5)$	632.45	0.5	54.83	0.1	17.32	0.05	15.49	0.12	2449.49	0.02
$(10, 0)$	2.45	0.4	1	0.6	0.1	0.5	0.04	0.8	17.32	0.4
$(30, 0)$	4	0.23	3.16	0.23	1.14	0.5	0.14	0.45	22.36	0.25
$(100, 0)$	10	0.13	4.9	0.13	2.45	0.35	1.41	0.3	24.49	0.15
$(300, 0)$	14.14	0.07	7.75	0.07	4	0.2	7.75	0.2	30	0.07
$(1000, 0)$	31.62	0.04	14.14	0.04	4	0.1	17.32	0.1	282.84	0.05
$(10, -0.347)$	4.47	0.4	2.45	0.5	1.9	0.4	0.04	0.8	7.75	0.4
$(30, -0.347)$	10	0.23	4.9	0.23	1.9	0.4	1.41	0.5	31.62	0.2
$(100, -0.347)$	12.65	0.13	10	0.13	6.32	0.13	10	0.3	34.64	0.15
$(300, -0.347)$	14.14	0.07	17.32	0.07	10	0.07	4.9	0.1	40	0.07
$(1000, -0.347)$	44.72	0.04	31.62	0.04	20	0.04	11.83	0.05	141.42	0.05
$(10, -1.151)$	10	0.4	7.75	0.4	6.32	0.4	2.45	0.5	4.47	0.4
$(30, -1.151)$	10	0.23	14.14	0.23	12.65	0.23	6.32	0.25	20	0.3
$(100, -1.151)$	20	0.13	25.46	0.13	24.49	0.13	8.94	0.15	44.72	0.3
$(300, -1.151)$	40	0.07	40	0.07	40	0.07	14.14	0.08	50	0.07
$(1000, -1.151)$	70.71	0.04	77.46	0.04	77.46	0.04	30	0.05	173.20	0.05
$(10, -1.844)$	10	0.4	14.14	0.4	14.14	0.4	4.47	0.4	6.32	0.4
$(30, -1.844)$	20	0.23	30	0.23	28.28	0.23	7.75	0.25	44.72	0.4
$(100, -1.844)$	28.28	0.13	48.99	0.13	54.77	0.13	17.32	0.15	44.72	0.3
$(300, -1.844)$	63.25	0.07	89.44	0.07	77.46	0.07	24.49	0.08	54.74	0.07
$(1000, -1.844)$	100	0.04	154.92	0.07	141.42	0.04	54.77	0.04	223.61	0.05

Then we computed 95% credible regions for the two parameters for each set of simulated data. For η, both equal-tail (ET) and shortest-length (SL) intervals were obtained. For the parameter $\mathbf{S}$, we used the cone-based credible sets provided by Bingham et al. (2009b) as described above. For the 95% credible regions for $\mathbf{S}$ and η, we found coverage rates for $\mathbf{S}$ and η (determining the proportion of simulation runs for which credible regions contained the true values). Results are given in Table 2. The most important outcome here is that just as for the previously published cases, the frequentist coverage rates of Bayes regions for both $\mathbf{S}$ and η for

every UARS distribution are consistent with their credible levels, and as sample size increases, the coverage rates converge more or less exactly to the nominal ones. This demonstrates that the Bayes approach is effective across the UARS class for obtaining good frequentist coverage accuracy.

Table 2 Coverage rates (%) for **S** and η using 95% Bayes credible regions. (Credible regions for η characterized here are ET intervals.)

	IG		Bunge		de la Valée Poussin		Lorentzian		wrapped Normal	
(n, η)	**S**	η	**S**	η	**S**	η	**S**	η	**S**	η
(10,1)	94.4	94.8	97.0	96.1	94.2	98.3	92.1	93.6	93.4	94
(30,1)	96.0	95.8	96.0	95.7	98.2	94.8	93.3	93.2	95.0	95.8
(100,1)	94.8	95.6	95.5	94.8	96.5	94.8	93.5	94.0	94.8	95.6
(300,1)	95.6	95.2	95.1	95.3	96.0	94.8	94.3	94.5	94.6	95.1
(1000,1)	95.2	95.0	95.1	95.2	95.5	94.9	94.5	94.7	94.9	95.0
$(10, 0.5)$	96.1	96.5	97.2	96.3	94.1	98.8	94.6	92.7	96.7	96.3
$(30, 0.5)$	98.0	96.7	95.0	96.1	95.6	97.8	95.5	93.4	97.0	95.7
$(100, 0.5)$	96.3	96.5	94.9	95.3	94.8	96.7	94.8	94.4	96.3	95.1
$(300, 0.5)$	95.7	95.3	95.1	94.9	94.8	94.6	95.3	95.5	94.5	94.8
$(1000, 0.5)$	95.1	95.1	95.1	95.1	95.2	94.9	95.1	95.4	95.1	95.2
$(10, 0)$	97.5	97.1	95.5	96.4	94.7	95.0	93.3	92.6	93.7	94.3
$(30, 0)$	95.0	95.9	96.0	96.7	93.7	94.3	94.5	95.1	93.9	94.2
$(100, 0)$	95.7	94.9	95.7	95.8	97.2	95.1	95.6	96.7	96.7	96.6
$(300, 0)$	95.5	94.9	95.1	95.5	95.7	96.5	95.1	95.8	95.3	94.7
$(1000, 0)$	95.3	95.0	95.3	95.3	94.8	95.1	95.4	95.1	95.0	95.1
$(10, -0.347)$	94.1	94.0	95.6	95.8	93.1	97.1	95.5	96.7	93.9	93.5
$(30, -0.347)$	98.0	97.8	93.0	93.9	97.4	97.0	95.9	96.6	94.0	94.8
$(100, -0.347)$	96.1	95.3	95.1	94.8	93.8	96.1	95.9	95.3	96.1	95.7
$(300, -0.347)$	95.3	95.5	95.3	94.8	95.1	96.3	95.0	95.6	95.4	94.9
$(1000, -0.347)$	95.1	95.4	95.1	95.0	95.2	94.9	95.0	94.9	94.9	95.1
$(10, -1.151)$	94.5	94.5	95.5	95.5	94.2	94.9	95.6	97.2	94.5	94.5
$(30, -1.151)$	93.0	93.3	95.0	95.7	94.9	94.7	93.6	94.8	93.8	94.4
$(100, -1.151)$	94.6	94.7	94.6	95.3	94.9	94.5	94.9	95.2	94.1	93.9
$(300, -1.151)$	94.9	94.8	94.9	95.0	95.0	95.2	95.5	95.1	94.7	95.6
$(1000, -1.151)$	94.9	95.0	95.0	95.0	95.0	95.2	94.9	94.9	94.8	95.2
$(10, -1.844)$	95.2	96.1	93.2	93.5	93.1	93.4	93.7	94.3	95.2	95.1
$(30, -1.844)$	93.2	93.0	97.5	96.9	94.0	94.6	94.0	94.6	94.2	95.0
$(100, -1.844)$	94.6	94.8	96.2	96.2	94.9	95.1	95.2	94.2	95.6	95.5
$(300, -1.844)$	95.0	95.2	95.1	94.9	94.6	94.8	95.2	94.9	95.0	94.9
$(1000, -1.844)$	94.9	95.0	95.0	94.9	95.0	95.1	95.3	94.7	94.9	94.9

We also considered median sizes for the 4,000 regions for **S** and η given in Tables 3 and 4. For all combinations (n, η), the equal-tail (ET) and shortest-length (SL) methods produce similar widths of 95% intervals for η, although the SL widths are somewhat smaller than the ET ones. Also (as one expects), for fixed η, as sample size n increases, the intervals become narrower. For fixed n, the median width of interval for η is monotone decreasing in η. (This is true in the present new simulations. Interestingly, strict monotonicity does not hold in the

wTN-UARS case and is almost surely related to the strong lack of monotonicity seen in the Jeffreys prior for this case. See Qiu et al. (2013) for details.)

Table 3 Median width of 95% Bayes credible intervals for η for both equal–tail (ET) and shortest-length (SL) intervals.

	IG		Bunge		de la Valée Poussin		Lorentzian		wrapped Normal	
(n, η)	ET Width	SL Width	ET Width	SL Width	ET Width	SL Width	ET Width	SL Width	ET Width	SL Width
(10,1)	1.987	1.956	1.979	1.748	1.909	1.710	1.981	1.765	0.513	0.509
(30,1)	0.696	0.680	0.888	0.765	1.740	1.504	0.943	0.908	0.288	0.279
(100,1)	0.583	0.564	0.551	0.448	1.256	1.071	0.510	0.508	0.143	0.129
(300,1)	0.368	0.359	0.405	0.315	1.254	1.058	0.423	0.421	0.072	0.063
(1000,1)	0.125	0.121	0.352	0.275	0.531	0.422	0.352	0.275	0.028	0.024
$(10, 0.5)$	0.822	0.810	1.559	1.369	1.312	1.277	1.777	1.547	0.523	0.519
$(30, 0.5)$	0.616	0.608	0.839	0.802	0.766	0.748	0.822	0.804	0.292	0.291
$(100, 0.5)$	0.381	0.377	0.490	0.485	0.340	0.304	0.400	0.398	0.152	0.139
$(300, 0.5)$	0.278	0.276	0.314	0.294	0.309	0.288	0.258	0.253	0.079	0.069
$(1000, 0.5)$	0.110	0.109	0.163	0.169	0.167	0.167	0.185	0.182	0.032	0.027
$(10, 0)$	0.797	0.767	1.509	1.342	1.166	1.155	1.771	1.530	0.522	0.521
$(30, 0)$	0.432	0.398	0.813	0.714	0.794	0.785	0.801	0.779	0.290	0.289
$(100, 0)$	0.173	0.172	0.180	0.179	0.179	0.179	0.425	0.423	0.162	0.160
$(300, 0)$	0.101	0.100	0.101	0.100	0.102	0.099	0.419	0.417	0.093	0.093
$(1000, 0)$	0.054	0.053	0.054	0.053	0.054	0.053	0.158	0.152	0.050	0.050
$(10, -0.347)$	0.562	0.553	0.564	0.555	0.566	0.555	1.920	1.679	0.527	0.525
$(30, -0.347)$	0.299	0.298	0.299	0.297	0.433	0.383	1.158	1.027	0.294	0.293
$(100, -0.347)$	0.163	0.163	0.166	0.165	0.163	0.163	0.901	0.897	0.164	0.164
$(300, -0.347)$	0.093	0.092	0.093	0.093	0.094	0.094	0.128	0.128	0.092	0.092
$(1000, -0.347)$	0.052	0.052	0.052	0.052	0.052	0.052	0.062	0.062	0.053	0.052
$(10, -1.151)$	0.544	0.539	0.543	0.539	0.542	0.537	1.843	1.275	0.528	0.527
$(30, -1.151)$	0.299	0.298	0.299	0.297	0.298	0.296	1.301	1.299	0.298	0.296
$(100, -1.151)$	0.163	0.163	0.163	0.163	0.163	0.163	0.165	0.163	0.163	0.163
$(300, -1.151)$	0.092	0.092	0.092	0.092	0.092	0.092	0.094	0.093	0.093	0.093
$(1000, -1.151)$	0.051	0.051	0.051	0.051	0.051	0.050	0.051	0.051	0.054	0.054
$(10, -1.844)$	0.542	0.538	0.543	0.538	0.540	0.536	0.540	0.536	0.524	0.523
$(30, -1.844)$	0.298	0.297	0.299	0.297	0.298	0.295	0.299	0.297	0.299	0.299
$(100, -1.844)$	0.163	0.162	0.163	0.162	0.162	0.162	0.154	0.163	0.163	0.162
$(300, -1.844)$	0.092	0.092	0.092	0.092	0.092	0.092	0.093	0.092	0.093	0.092
$(1000, -1.844)$	0.050	0.050	0.051	0.051	0.051	0.051	0.050	0.050	0.056	0.056

As mentioned before, the size of a cone-based credible region for $\mathbf{S}$ is characterized by the angle defining the conic regions. For fixed η, the median angle decreases as n increases. The empirical convergence rate (found by regressing the log of median angle over the log of n for $n = 100, 300, 1000$) is approximately $O(1/\sqrt{n})$ for regular cases, consistent with the smoothness of their likelihood functions, and approximately $O(1/n)$ for the wN-UARS distribution, consistent with the fact that its likelihood function has singularities. (The credible regions for $\mathbf{S}$ of wN-UARS distributions have qualitatively the same behavior as those for the vM-UARS distribution (Bingham et al. 2009b).) For details of the rate issue for Bayes methods in non-regular models of this type, see Nordman et al. (2009).

The Bayes results for regular cases here essentially match those reported by Bingham et

Table 4 Median cone angle of Bayes credible sets for $\mathbf{S}$ with different combinations (n, η) and the apparent moderate sample size convergence rate (ACR) of the median angles for fixed η.

	IG		Bunge		de la Vallée Poussin		Lorentzian		wrapped Normal	
(n, η)	Angle	ACR	Angle	ACR	Angle	ACR	Angle	ACR	Angle	ACR
(10,1)	1.131		1.131		1.077		1.541		0.925	
(30,1)	0.410		0.397		0.405		0.535		0.405	
(100,1)	0.034	$n^{-0.576}$	0.033	$n^{-0.562}$	0.040	$n^{-0.563}$	0.051	$n^{-0.536}$	0.023	$n^{-1.053}$
(300,1)	0.016		0.015		0.026		0.039		0.004	
(1000,1)	0.009		0.009		0.011		0.015		0.002	
$(10, 0.5)$	1.536		1.583		1.542		1.547		0.163	
$(30, 0.5)$	1.521		1.530		1.536		1.543		0.057	
$(100, 0.5)$	1.477	$n^{-0.501}$	1.522	$n^{-0.498}$	1.529	$n^{-0.534}$	0.549	$n^{-0.527}$	0.018	$n^{-0.957}$
$(300, 0.5)$	1.246		1.261		1.322		0.250		0.008	
$(1000, 0.5)$	0.471		0.489		0.453		0.162		0.002	
$(10, 0)$	1.354		1.420		1.571		1.547		0.285	
$(30, 0)$	0.869		1.015		1.554		1.541		0.086	
$(100, 0)$	0.396	$n^{-0.500}$	0.461	$n^{-0.520}$	0.512	$n^{-0.503}$	0.545	$n^{-0.504}$	0.046	$n^{-1.040}$
$(300, 0)$	0.231		0.250		0.459		0.290		0.010	
$(1000, 0)$	0.125		0.139		0.163		0.158		0.004	
$(10, -0.347)$	0.732		0.751		0.778		1.535		0.430	
$(30, -0.347)$	0.403		0.411		0.571		1.465		0.083	
$(100, -0.347)$	0.230	$n^{-0.527}$	0.230	$n^{-0.510}$	0.406	$n^{-0.539}$	0.312	$n^{-0.504}$	0.056	$n^{-1.04}$
$(300, -0.347)$	0.125		0.130		0.210		0.140		0.009	
$(1000, -0.347)$	0.069		0.071		0.117		0.097		0.005	
$(10, -1.151)$	0.292		0.300		0.571		0.831		0.616	
$(30, -1.151)$	0.163		0.164		0.303		0.446		0.045	
$(100, -1.151)$	0.091	$n^{-0.527}$	0.092	$n^{-0.516}$	0.094	$n^{-0.510}$	0.246	$n^{-0.515}$	0.014	$n^{-1.149}$
$(300, -1.151)$	0.048		0.049		0.047		0.135		0.005	
$(1000, -1.151)$	0.027		0.028		0.029		0.075		0.001	
$(10, -1.844)$	0.143		0.144		0.571		0.461		0.504	
$(30, -1.844)$	0.080		0.081		0.080		0.078		0.048	
$(100, -1.844)$	0.045	$n^{-0.509}$	0.042	$n^{-0.509}$	0.043	$n^{-0.490}$	0.041	$n^{-0.505}$	0.012	$n^{-1.07}$
$(300, -1.844)$	0.029		0.024		0.030		0.038		0.002	
$(1000, -1.844)$	0.014		0.013		0.014		0.013		0.001	

al. (2010b) for the (regular) symmetric Matrix Fisher distribution, that were found to be comparable to maximum likelihood results. For non-regular cases (for the new wN-UARS model), simulations in Bingham et al. (2009b) and Qiu et al. (2013) for the (non-regular) vM-UARS and wTN-UARS models agree with findings here as well. (Note that for the vM-UARS case, the published work demonstrates that the Bayes methodology is completely superior to pseudo-likelihood methods.)

5 Discussion

Between this paper and the existing literature (Bingham et al. 2009b, Bingham et al. 2010a, and Qiu et al. 2013), we have established a complete one-sample non-informative Bayes methodology which is reasonable and effective for 8 parametric UARS symmetric distributions for 3-D rotations, 5 that are regular statistical models and 3 that are non-regular models.

Bingham et al. (2009b) demonstrated the possiblity of Bayes one-way random effects analyses and Bingham et al. (2010b) demonstrated the possibility of Bayes analysis of hierarchical models for the vM-UARS class that can easily be extened to all classes discussed here. Indeed, any of the 8 basic UARS models discussed here can serve as components of the kind of multi-level hierarchical model employed there. And Bingham et al.(2012) has opened a line of inquiry demonstrating how the basic UARS construction and distributions and non-informative priors can be used in Bayes analyses where classes of non-symmetric distributions are needed. The 8 basic forms and priors considered here become essential components for these more complicated and richer structures.

Because the UARS class has wide usefulness, our next step will be the development of an `R` package implementing non-informative Bayes one-sample methods for the UARS class.

Appendix

This note contains of details of calculations of Fisher information functions for all existing UARS angular distributions.

A Isotropic Gaussian Angular Distribution

Let $f(r|m,\kappa) = (2m+1)\exp\left[-m(m+1)/(2\kappa^2)\right]\frac{\sin[(m+1/2)r]}{\sin(r/2)}, C_{IG}(r|\kappa) = \frac{1-\cos r}{2\pi}\sum\limits_{m=0}^{\infty} f(r|m,\kappa)$. So

$$\frac{d}{d\kappa}\log(C_{IG}(r|\kappa)) = \frac{\sum\limits_{m=0}^{\infty}\frac{d}{d\kappa}f(r|m,\kappa)}{\sum\limits_{m=0}^{\infty} f(r|m,\kappa)} = \frac{\sum\limits_{m=0}^{\infty}\left(m(m+1)/\kappa^3\right)f(r|m,\kappa)}{\sum\limits_{m=0}^{\infty} f(r|m,\kappa)},$$

and

$$\begin{aligned}\frac{d^2}{d\kappa^2}\log(C_{IG}(r|\kappa)) &= \frac{\sum\limits_{m=0}^{\infty}\left(-3m(m+1)/\kappa^4\right)f(r|m,\kappa) + \sum\limits_{m=0}^{\infty}(m^2(m+1)^2/\kappa^6)f(r|m,\kappa)}{\sum\limits_{m=0}^{\infty} f(r|m,\kappa)} \\ &\quad - \frac{\left(\sum\limits_{m=0}^{\infty}\left(m(m+1)/\kappa^3\right)f(r|m,\kappa)\right)^2}{\left(\sum\limits_{m=0}^{\infty} f(r|m,\kappa)\right)^2}.\end{aligned}$$

Then

$$\begin{aligned}
\mathcal{I}_{IG}(\kappa) &= -E\left[\frac{d^2}{d\kappa^2}\log(C_{IG}(r|\kappa))\right] = -\int_{-\pi}^{\pi}\frac{d^2}{d\kappa^2}\log(C_{IG}(r|\kappa))\times\frac{1-\cos r}{2\pi}\sum_{m=0}^{\infty}f(r|m,\kappa)dr \\
&= \frac{1}{\kappa^6}\int_{-\pi}^{\pi}\frac{1-\cos r}{2\pi}\frac{\left[\sum_{m=0}^{\infty}m(m+1)f(r|m,\kappa)\right]^2}{\sum_{m=0}^{\infty}f(r|m,\kappa)}dr \\
&\quad -\frac{1}{\kappa^6}\int_{-\pi}^{\pi}\frac{1-\cos r}{2\pi}\sum_{m=0}^{\infty}\left[m^2(m+1)^2-3m(m+1)\kappa^2\right]f(r|m,\kappa)dr.
\end{aligned}$$

B Bunge Angular Distribution

First $\frac{d}{d\kappa}\log(C_{Bunge}(r|\kappa)) = -\kappa r^2 + \frac{d}{d\kappa}\log N(\kappa)$, so

$$\frac{d^2}{d\kappa^2}\log(C_{Bunge}(r|\kappa)) = -r^2 + \frac{d^2}{d\kappa^2}\log N(\kappa).$$

Thus

$$\begin{aligned}
\mathcal{I}_{Bunge}(\kappa) &= -E\left[\frac{d^2}{d\kappa^2}\log(C_{Bunge}(r|\kappa))\right] \\
&= E(r^2) - \frac{d^2\log(N(\kappa))}{d\kappa^2}.
\end{aligned}$$

C de la Vallée Poussin Angular Distribution

First, $\frac{d^2}{d\kappa^2}\log(C_{Poussin}(r|\kappa)) = 8\log(\cos(r/2)) - \frac{d^2}{d\kappa^2}\log B(3/2, 2\kappa^2+1/2)$. Now, the derivative of the beta function is $\frac{\partial}{\partial b}B(a,b) = B(a,b)\left[\psi_0(b)-\psi_0(a+b)\right]$ and the derivative of the digamma function $\psi_0(z)$ is $\frac{d}{dz}\psi_0(z) = \psi_1(z)$ where $\psi_1(z)$ is the trigamma function. Then

$$\begin{aligned}
\frac{d^2}{d\kappa^2}\log B(3/2, 2\kappa^2+1/2) &= \frac{d}{d\kappa}\left\{\frac{d\left[\log B(3/2,2\kappa^2+1/2)\right]}{d(2\kappa^2+1/2)}\cdot\frac{d(2\kappa^2+1/2)}{d\kappa}\right\} \\
&= \frac{d}{d\kappa}\left\{\frac{d\left[B(3/2,2\kappa^2+1/2)\right]}{d(2\kappa^2+1/2)}\frac{4\kappa}{B(3/2,2\kappa^2+1/2)}\right\} \\
&= \frac{d}{d\kappa}\left\{4\kappa\left[\psi_0(2\kappa^2+1/2)-\psi_0(2\kappa^2+2)\right]\right\} \\
&= 4\left[\psi_0(2\kappa^2+1/2)-\psi_0(2\kappa^2+2)\right] + 16\kappa^2\left[\psi_1(2\kappa^2+1/2)-\psi_1(2\kappa^2+2)\right].
\end{aligned}$$

Thus

$$\begin{aligned}\mathcal{I}_{Poussin}(\kappa) &= -E\left\{\frac{d^2}{d\kappa^2}\log\left[C_{Poussin}(r|\kappa)\right]\right\} \\ &= 4\left[\psi_0(2\kappa^2+1/2)-\psi_0(2\kappa^2+2)\right]+16\kappa^2\left[\psi_1(2\kappa^2+1/2)-\psi_1(2\kappa^2+2)\right]-8E\left\{\log\left[\cos(r/2)\right]\right\},\end{aligned}$$

where ψ_n is the polygamma function.

D Lorentzian Angular Distribution

First

$$\frac{d\log C_{Lorentzian}(r|\lambda)}{d\kappa}=\frac{d\log C_{Lorentzian}(r|\lambda)}{d\lambda}\frac{d\lambda}{d\kappa}=\frac{C'_{Lorentzian}(r|\lambda)}{C_{Lorentzian}(r|\lambda)}\left[1/2-4/(\kappa+2)^3\right],$$

and

$$\begin{aligned}\frac{d^2\log C_{Lorentzian}(r|\lambda)}{d\kappa^2} &= \frac{C''_{Lorentzian}(r|\lambda)C_{Lorentzian}(r|\lambda)-\left[C'_{Lorentzian}(r|\lambda)\right]^2}{\left[C_{Lorentzian}(r|\lambda)\right]^2}\left[1/2-4/(\kappa+2)^3\right]^2 \\ &\quad+\frac{12}{(\kappa+2)^4}\frac{C'_{Lorentzian}(r|\lambda)}{C_{Lorentzian}(r|\lambda)}.\end{aligned}$$

Thus

$$\begin{aligned}\mathcal{I}_{Lorentzian}(\kappa) &= -\frac{12}{(\kappa+2)^4}\int_{-\pi}^{\pi}C'_{Lorentzian}(r|\lambda)dr-\left[1/2-4/(\kappa+2)^3\right]^2\int_{-\pi}^{\pi}C''_{Lorentzian}(r|\lambda)dr \\ &\quad+\left[1/2-4/(\kappa+2)^{-3}\right]^2\int_{-\pi}^{\pi}\frac{\left[C'_{Lorentzian}(r|\lambda)\right]^2}{C_{Lorentzian}(r|\lambda)}dr.\end{aligned}$$

E Matrix Fisher Angular Distribution

First, $\frac{d^2}{d\kappa^2}\log\left[C_{MF}(r|\kappa)\right] = 2\cos r - \frac{d^2}{d\kappa^2}\log\left[I_0(\kappa^2) - I_1(\kappa^2)\right]$. The derivatives of the modified Bessel functions are $\frac{d}{d\kappa}I_0(\kappa^2) = 2\kappa I_1(\kappa^2)$, $\frac{d}{d\kappa}I_1(\kappa^2) = 2\kappa(I_0(\kappa^2) - I_1(\kappa^2)/\kappa^2)$. Then

$$\begin{aligned}
\frac{d^2}{d\kappa^2}\log\left[I_0(\kappa^2) - I_1(\kappa^2)\right] &= \frac{d}{d\kappa}\left[\frac{2\kappa I_1(\kappa^2) - 2\kappa I_0(\kappa^2) + 2I_1(\kappa^2)/\kappa}{I_0(\kappa^2) - I_1(\kappa^2)}\right] \\
&= \frac{d}{d\kappa}\left[-2\kappa + \frac{2I_1(\kappa^2)}{\kappa I_0(\kappa^2) - \kappa I_1(\kappa^2)}\right] \\
&= -2 + \frac{2\kappa\left[I_0(\kappa^2) - I_1(\kappa^2)\right]\left[2\kappa(I_0(\kappa^2) - I_1(\kappa^2)/\kappa^2)\right]}{\kappa^2\left[I_0(\kappa^2) - I_1(\kappa^2)\right]^2} \\
&\quad - \frac{2I_1(\kappa^2)\left[I_0(\kappa^2) - I_1(\kappa^2) + 2\kappa^2(I_1(\kappa^2) - I_0(\kappa^2) + I_1(\kappa^2)/\kappa^2)\right]}{\kappa^2\left[I_0(\kappa^2) - I_1(\kappa^2)\right]^2} \\
&= -2 + \frac{4\left[I_0(\kappa^2) + I_1(\kappa^2)\right]}{I_0(\kappa^2) - I_1(\kappa^2)} + \frac{2I_1^2(\kappa^2) - 6I_0(\kappa^2)I_1(\kappa^2)}{\kappa^2\left[I_0(\kappa^2) - I_1(\kappa^2)\right]^2}.
\end{aligned}$$

Thus

$$\mathcal{I}_{MF}(\kappa) = -2E\left(\cos r\right) - 2 + \frac{2I_1^2(\kappa^2) - 6I_1(\kappa^2)I_0(\kappa^2)}{\kappa^2\left[I_0(\kappa^2) - I_1(\kappa^2)\right]^2} + \frac{4\left[I_0(\kappa^2) + I_1(\kappa^2)\right]}{I_0(\kappa^2) - I_1(\kappa^2)}.$$

F Wrapped Normal Angular Distribution

Let $g(r|m,\kappa) = \exp\left[-(2m\pi - r)^2\kappa^2/2\right]$, $\frac{\partial g(r|m,\kappa)}{\partial\kappa} = -(2m\pi - r)^2\kappa g(r|m,\kappa)$. Then

$$\frac{d\log C_{wN}(r|\kappa)}{d\kappa} = \frac{1}{\kappa} + \frac{\sum_{m=-\infty}^{\infty} -(2m\pi - r)^2\kappa g(r|m,\kappa)}{\sum_{m=-\infty}^{\infty} g(r|m,\kappa)},$$

and

$$\begin{aligned}
\frac{d^2\log C_{wN}(r|\kappa)}{d\kappa^2} &= \frac{-1}{\kappa^2} + \frac{\sum_{m=-\infty}^{\infty} -(2m\pi - r)^2 g(r|m,\kappa) + \sum_{m=-\infty}^{\infty}\kappa^2(2m\pi - r)^4 g(r|m,\kappa)}{\sum_{-\infty}^{\infty} g(r|m,\kappa)} \\
&\quad - \frac{\kappa^2\left[\sum_{-\infty}^{\infty}(2m\pi - r)^2 g(r|m,\kappa)\right]^2}{\left[\sum_{-\infty}^{\infty} g(r|m,\kappa)\right]^2}.
\end{aligned}$$

Thus

$$\begin{aligned}\mathcal{I}_{wN}(\kappa) &= \frac{1}{\kappa^2}+\frac{\kappa}{\sqrt{2\pi}}\int_{-\pi}^{\pi}\sum_{m=-\infty}^{\infty}(2m\pi-r)^2 g(r|m,\kappa)dr-\frac{\kappa^3}{\sqrt{2\pi}}\int_{-\pi}^{\pi}\sum_{-\infty}^{\infty}(2m\pi-r)^4 g(r|m,\kappa)dr \\ &+ \frac{\kappa^3}{\sqrt{2\pi}}\int_{-\pi}^{\pi}\frac{\left[\sum_{-\infty}\infty(2m\pi-r)^2 g(r|m,\kappa)\right]^2}{\sum_{-\infty}^{\infty}g(r|m,\kappa)}dr.\end{aligned}$$

G von-Mises Angular Distribution

First $\frac{d^2}{d\kappa^2}\log\left[C_{MF}(r|\kappa)\right]=2\cos r-\frac{d^2\log I_0(\kappa^2)}{d\kappa^2}$. Following the results quoted above concerning the derivatives of the Bessel functions, we have

$$\begin{aligned}\frac{d^2\log I_0(\kappa^2)}{d\kappa^2} &= \frac{d}{d\kappa}\left[\frac{2\kappa I_1(\kappa^2)}{I_0(\kappa^2)}\right] \\ &= \frac{2I_1(\kappa^2)}{I_0(\kappa^2)}+2\kappa\frac{2\kappa I_0(\kappa^2)\left[I_0(\kappa^2)-I_1(\kappa^2)/\kappa^2\right]-2\kappa\left[I_1(\kappa^2)\right]^2}{\left[I_0(\kappa^2)\right]^2} \\ &= 4\kappa^2-\frac{2I_0(\kappa^2)}{I_1(\kappa^2)}-4\kappa^2\frac{I_0^2(\kappa^2)}{I_1^2(\kappa^2)}.\end{aligned}$$

Thus

$$\mathcal{I}_{vM}(\kappa)=-2E\left(\cos r\right)-4\kappa^2\frac{I_1^2(\kappa^2)}{I_0^2(\kappa^2)}-\frac{2I_1(\kappa^2)}{I_0(\kappa^2)}+4\kappa^2.$$

H Wrapped Trivariate Normal Angular Distribution

Let $g(r|m)=(2m\pi-r)^2$, then

$$\begin{aligned}\frac{d^2}{d\kappa^2}\log C_(wTN)(r|\kappa) &= \frac{d}{d\kappa}\left\{\frac{3}{\kappa}-\kappa\frac{\sum_{m=-\infty}^{\infty}g^2(r|m)\exp\left[-\kappa^2 g(r|m)/2\right]}{\sum_{m=-\infty}^{\infty}g(r|m)\exp\left[-\kappa^2 g(r|m)/2\right]}\right\} \\ &= -\frac{3}{\kappa^2}-\frac{\sum_{m=-\infty}^{\infty}g^2(r|m)\exp\left[-\kappa^2 g(r|m)/2\right]}{\sum_{m=-\infty}^{\infty}g(r|m)\exp\left[-\kappa^2 g(r|m)/2\right]} \\ &+ \kappa^2\left[\frac{\sum_{m=-\infty}^{\infty}g^3(r|m)\exp\left[-\kappa^2 g(r|m)/2\right]}{\sum_{m=-\infty}^{\infty}g(r|m)\exp\left[-\kappa^2 g(r|m)/2\right]}-\left(\frac{\sum_{m=-\infty}^{\infty}g^2(r|m)\exp\left[-\kappa^2 g(r|m)/2\right]}{\sum_{m=-\infty}^{\infty}g(r|m)\exp\left[-\kappa^2 g(r|m)/2\right]}\right)^2\right]\end{aligned}$$

Thus

$$\begin{aligned}
\mathcal{I}_{wTN}(\kappa) &= \frac{3}{\kappa^2} + \int_0^\pi \sum_{m=-\infty}^{\infty} \frac{\kappa^3}{\sqrt{2\pi}} g^2(r|m) \exp\left[-\kappa^2 g(r|m)/2\right] dr \\
&\quad - \int_0^\pi \sum_{m=-\infty}^{\infty} \frac{\kappa^5}{\sqrt{2\pi}} g^3(r|m) \exp\left[-\kappa^2 g(r|m)/2\right] dr \\
&\quad + \int_0^\pi \frac{\kappa^5}{\sqrt{2\pi}} \frac{\left\{\sum_{m=-\infty}^{\infty} g^2(r|m) \exp\left[-\kappa^2 g(r|m)/2\right]\right\}^2}{\sum_{m=-\infty}^{\infty} g(r|m) \exp\left[-\kappa^2 g(r|m)/2\right]} dr \\
&= \frac{3}{\kappa^2} + E(g(r|m)) - \kappa^2 E(g^2(r|m)) + \int_0^\pi \frac{\kappa^5}{\sqrt{2\pi}} \frac{\left\{\sum_{m=-\infty}^{\infty} g^2(r|m) \exp\left[-\kappa^2 g(r|m)/2\right]\right\}^2}{\sum_{m=-\infty}^{\infty} g(r|m) \exp\left[-\kappa^2 g(r|m)/2\right]} dr \\
&= \frac{3}{\kappa^2} + \frac{3}{\kappa^2} - \kappa^2 \times \frac{15}{\kappa^4} + \int_0^\pi \frac{\kappa^5}{\sqrt{2\pi}} \frac{\left\{\sum_{m=-\infty}^{\infty} g^2(r|m) \exp\left[-\kappa^2 g(r|m)/2\right]\right\}^2}{\sum_{m=-\infty}^{\infty} g(r|m) \exp\left[-\kappa^2 g(r|m)/2\right]} dr \\
&= -\frac{9}{\kappa^2} + \frac{\kappa^5}{\sqrt{2\pi}} \int_{-\pi}^\pi \frac{\left\{\sum_{m=-\infty}^{\infty} g^2(r|m) \exp\left[-\kappa^2 g(r|m)/2\right]\right\}^2}{\sum_{m=-\infty}^{\infty} g(r|m) \exp\left[-\kappa^2 g(r|m)/2\right]} dr.
\end{aligned}$$

Bibliography

[1] Bingham, M.A., Nordman, D.J., Vardeman, S.B., 2009a. Modeling and Inference for Measured Crystal Orientations and a Tractable Class of Symmetric Distributions for Rotations in Three Dimensions. *Journal of the American Statistical Association* 104, 1385-1397.

[2] Bingham, M.A., Vardeman, S.B., Nordman, D.J., 2009b. Bayes One-Sample and One-Way Random Effects Analyses for 3-D Orientations with Application to Materials Science. *Bayesian Analysis* 4, 607-630.

[3] Bingham, M.A., Nordman, D.J., Vardeman, S.B., 2010a. Finite-Sample Investigation of Likelihood and Bayes Inference for the Symmetric von Mises-Fisher Distribution. *Computational Statistics and Data Analysis* 54, 1317-1327.

[18] Bingham, M.A., Lograsso, B.K., Laabs, F.C., 2010b. A Statistical Analysis of the Variation in Measured Crystal Orientations Obtained Through Electron Backscatter Diffraction. *Ultramicroscopy* 110, 1312-1319.

[18] Bingham, M.A., Nordman, D.J., Vardeman, S.B., 2012. *Journal of Agricultural, Biological, and Environmental Statistics*, Vol. 17, No. 4, 527-543.

[18] Borovkov, M., Savyolova, T., 2007. The Computational Approaches to Calculate Normal Distributions on the Rotation Group. *Journal of Applied Crystallography* 40, 449-455.

[7] Bunge, H.J., 1982. *Texture Analysis in Materials Science*. Butterworth, London.

[8] Chang, T., Rivest, L.-P., 2001. M-Estimation for Location and Regression Parameters in Group Models: A Case Study Using Stiefel Manifolds. *Annals of Statistics* 29, 784-814.

[9] Downs, T.D., 1972. Orientation Statistics. *Biometrika* 59, 665-676.

[10] Jupp, P.E., Mardia, K.V., 1979. Maximum Likelihood Estimators for the Matrix Von Mises-Fisher and Bingham Distributions. *Annals of Statistics* 7, 599-606.

[7] León, C.A., Massé, J.-C., Rivest, L.-P., 2006. A Statistical Model for Random Rotations. *Journal of Multivariate Analysis* 97, 412-430.

[8] Matthies, S., 1982. Form Effects in the Description of the Orientation Distribution Function (ODF) of Texturized Materials by Model Components. *Physica Status Solidi (b)* 112, 705-716.

[9] Matthies, S., Muller, J., Vinel, G.W., 1988. On the Normal Distribution in the Orientation Space. *Textures and Microstructures* 10, 77-96.

[18] Nikolayev D.I., Savyolova, T.I., 1997. Normal Distribution on the Rotation Group $SO(3)$. *Textures and Microstructures* 29, 201-233.

[15] Nordman, D.J., Vardeman, S.B., Bingham, M.A., 2009. Uniformly Hyper-efficient Bayes Inference in a Class of Non-regular Problems. *The American Statistician* 63, 234-238.

[16] Oualkacha, K., Rivest, L.-P., 2008. A New Statistical Model for Random Unit Vectors. *Journal of Multivariate Analysis* 100, 70-80.

[12] Savyolova, T.I., 1985. Preface to *Novye Metody Issledovanija Tekstury Polikristalliĉeskich Materialov*. Metallurgija, Moscow.

[18] Schaeben, H., 1992. "Normal" orientation distributions. *Textures and Microstructures* 19, 197-202.

[13] Schaeben, H., 1997. The de la Vallée Poussin Standard Orientation Density Function. *Textures and Microstructures* 33, 365-373.

[10] Qiu, Y., Nordman, D.J., Vardeman, S.B., 2013. A Wrapped Trivariate Normal Distribution for 3-D Rotations and Bayes Inference. Under review by *Statistic Sinica*.

CHAPTER 4. UARSBAYES: AN R PACKAGE FOR 3-D ORIENTATION DATA

A paper submitted to *R Journal*

Yu Qiu and Melissa A. Bingham

Abstract

The **uarsbayes** package for R provides tools for generating 3-D orientation data from symmetric Uniform Axis-Random Spin (UARS) models. The package will also perform one-sample Bayes inference with non-informative priors, which includes simulating values from the posterior and generating a graphical display of cones that serve as a credible region for the central orientation of the distribution. Q-Q plots can be constructed using the **uarsbayes** package to perform goodness-of-fit for various members of the UARS class.

1 Introduction

Three-dimensional orientation data often arise in areas such as materials science and human kinematics. Despite the fact that several new statistical models have been developed for orientation data over the recent years, there is little software available to practicioners for using such models. The R package **uarsbayes** implements the Uniform Axis-Random Spin (UARS) class introduced by Bingham, Nordman and Vardeman (2), which views 3-D orientations as directionally symmetric random rotational perturbations around some central orientation. The package **uarsbayes** also provides one-sample Bayes analyses with non-informative priors for random 3-D orientation data, which have been demonstrated to be effective and attractive

(Bingham, Vardeman and Nordman (3); Bingham, Lograsso and Laabs (1); Qiu, Nordman and Vardeman (10); Qiu, Nordman and Vardeman (11)).

The article is organized as follows. The statistical models and the Bayes methods implemented in the **uarsbayes** package are first reviewed. Then, the capacity of the **uarsbayes** package is demonstrated with a real data example from an electron backscatter diffraction (EBSD) experiment. Finally, some concluding remarks are provided at the end.

2 UARS Models for 3-D Orientation Data

Bingham, Nordman and Vardeman (2) described the general construction and expression of the UARS class of distributions. By rotating an identity matrix $\mathbf{I}_{3\times 3}$ about a uniformly distributed axis $\mathbf{u} = (u1, u2, u3)^T$ through a random angle $r \in (-\pi, \pi]$, where r has a symmetric density $C(r|\kappa)$ with spread controlled by the concentration parameter $\kappa > 0$, we obtain a random UARS rotation with mean direction $\mathbf{I}_3$ as follows

$$\begin{aligned}\mathbf{M}(r,\mathbf{u}) &\equiv \mathbf{u}\mathbf{u}^T + (\mathbf{I}_{3\times 3} - \mathbf{u}\mathbf{u}^T)\cos r \\ &+ \begin{pmatrix} 0 & -u_3 & u_2 \\ u_3 & 0 & -u_1 \\ -u_2 & u_1 & 0 \end{pmatrix} \sin r.\end{aligned}$$

Then a UARS observation $\mathbf{O}$ with mean rotation $\mathbf{S} \in SO(3)$ (i.e., the set of an orthogonal matrices with determinant 1) is defined as $\mathbf{O} = \mathbf{S} \cdot \mathbf{M}(r, \mathbf{u})$, representing a directionally symmetric perturbation of a central location parameter $\mathbf{S}$. The density of the UARS observation $\mathbf{O}$ can be expressed with respect to the uniform distribution on $SO(3)$ as

$$f(\mathbf{O}|\mathbf{S}, \kappa) = \frac{4\pi}{3 - tr(\mathbf{S}^T\mathbf{O})} C(\arccos[2^{-1}(tr(\mathbf{S}^T\mathbf{O}) - 1)]|\kappa), \tag{1}$$

where $tr(\cdot)$ and $(\cdot)^T$ denote the matrix trace and transpose, respectively.

The density of any distribution in the UARS class is completely determined by the angular density, $C(r|\kappa)$. If $\lim_{r\to 0} \frac{C(r|\kappa)}{1-\cos r}$ is not finite, (1) is unbounded at $\mathbf{O} = \mathbf{S}$. So in the following

discussion, we list existing angular densities organized by the behavior of $\lim_{r\to 0} \frac{C(r|\kappa)}{1-\cos r}$.

2.1 Regular Cases

For these distributions, $\lim_{r\to 0} \frac{C(r|\kappa)}{1-\cos r}$ is finite. We use κ to represent the concentration parameters for all regular distributions. With the exception of Lorentzian case, these distributions become essentially identical as $\kappa \to \infty$.

2.1.1 Isotropic Gaussian Angular Distribution

The density for the isotropic Gaussian angular distribution is

$$\begin{aligned} C_{IG}(r|\kappa) &= \frac{1-\cos r}{2\pi} \sum_{m=0}^{\infty} (2m+1) \exp\left[-m(m+1)/(2\kappa^2)\right] \\ &\times \frac{\sin\left[(m+1/2)r\right]}{\sin(r/2)}; \end{aligned}$$

(Matthies, Muller and Vinel (9); Savyolova (12)). In **uarsbayes** this density can be evaluated using `diG(r,k)` and the samples of the angles can be generated using `riG(n,k)`.

2.1.2 Bunge's Gaussian Angular Distribution

The density for the Bunge's Gaussian angular distribution is

$$C_{Bunge}(r|\kappa) = \frac{1-\cos r}{2\pi} N(\kappa) \exp\left[-\kappa^2 r^2/2\right];$$

with a normalizing constant $N(\kappa)$ (Bunge (5)). In **uarsbayes** this density can be evaluated using `dbunge(r,k)` and the samples of the angles can be generated using `rbunge(n,k)`.

2.1.3 de la Vallée Poussin Angular Distribution

The density for the de la Vallée Poussin angular distribution is

$$C_{Poussin}(r|\kappa) = \frac{1-\cos r}{2\pi} \frac{B(3/2,1/2)}{B(3/2,2\kappa^2+1/2)} \cos^{4\kappa^2}(r/2);$$

(Schaeben (13)). León, Massé and Rivest (7) later derived the same distribution, calling it the Cayley distribution and providing an equivalent form for the density

$$C_{Cayley}(r|\kappa) = \frac{1-\cos r}{2\pi}\frac{\sqrt{\pi}\Gamma(2\kappa^2+2)(1+\cos r)^{2\kappa^2}}{2^{2\kappa^2}\Gamma(2\kappa^2+1/2)}.$$

In **uarsbayes** this density can be evaluated using `dpoussin(r,k)` and samples of the angles can be generated using `rpoussin(n,k)`.

2.1.4 Lorentzian Angular Distribution

The density for the Lorentzian angular distribution is

$$\begin{aligned} C_{Lorentzian}(r|\kappa) &= \frac{1-\cos r}{2\pi}(1+\lambda) \\ &\times \frac{(1+2\lambda)^2+4\lambda(\lambda+1)\cos^2(r/2)}{\left[(1+2\lambda)^2-4\lambda(\lambda+1)\cos^2(r/2)\right]^2}; \end{aligned}$$

(Matthies (8)). Letting $\lambda = \kappa/2 - 0.5 + 2/(\kappa+2)^2$ puts the Lorentzian distribution on roughly the same scale as the others, but the Lorentzian shape differs from the other distributions given here for large κ. In **uarsbayes** this density can be evaluated using `dloren(r,k)` and samples of the angles can be generated using `rloren(n,k)`.

2.1.5 Matrix Fisher Angular Distribution

The density for the matrix Fisher (MF) angular distribution is

$$C_{MF}(r|\kappa) = \frac{1-\cos r}{2\pi}\frac{\exp(\kappa^2\cos r)}{I_0(\kappa^2)-I_1(\kappa^2)};$$

where I_i denotes the modified Bessel function of order i. In **uarsbayes** this density can be evaluated using `dmf(r,k)` and samples of the angles can be generated using `rmf(n,k)`.

2.2 Non-regular Cases

For these angular distributions, $\lim_{r\to 0} \frac{C(r|\kappa)}{1-\cos r}$ is infinite and the UARS density (1) has a singularity at $\mathbf{O} = \mathbf{S}$.

2.2.1 Wrapped Normal Angular Distribution

The density for the wrapped Normal (wNM) angular distribution is

$$C_{wNM}(r|\kappa) = \frac{\kappa}{\sqrt{(2\pi)}} \sum_{m=-\infty}^{\infty} \exp\left(-(2m\pi - r)^2\kappa^2/2\right).$$

In **uarsbayes** this density can be evaluated using `dwnorm(r,k)` and samples of the angles can be generated using `rwnorm(n,k)`.

2.2.2 Von-Mises Angular Distribution

To be consistent with the wrapped normal angular density, the density for the von-Mises (vM) angular distribution is parameterized as

$$C_{vM}(r|\kappa) = \frac{\exp(\kappa^2\cos(r))}{2\pi I_0(\kappa^2)}.$$

We use the existing density function `dvm(r,mu,k)` in the package **CircStats** with κ^2. In **uarsbayes** this density can be evaluated using `dvm(r,0,`k^2`)` and samples of the angles can be generated using `rvm(n,0,`k^2`)`.

2.2.3 Wrapped Trivariate Normal Angular Distribution

The density for the wrapped Trivariate Normal (wTN) angular distribution is

$$C_{wTN}(r|\kappa) = \sum_{m=-\infty}^{\infty} \frac{\kappa^3}{\sqrt{2\pi}}(2m\pi - r)^2 \exp\left[-\kappa^2(2m\pi - r)^2/2\right]$$

(Qiu, Nordman and Vardeman (10)). In **uarsbayes** this density can be evaluated using `dwtn(r,k)` and samples of the angles can be generated using `rwtn(n,k)`.

Inserting the angular densities given above into (1), we obtain different members of the UARS class. In **uarsbayes** the UARS rotations can be generated using

```
ruars(n,S,k,model)
```

where `model` can be specified as any of the listed distributions above, the argument `S` is a 3×3 matrix representing the central location, the argument `k` represents the concentration parameter, and the argument `n` represents the size of the desired dataset. The function will return a $9 \times n$ matrix with each column standing for one generated 3×3 UARS rotation (taken by column).

3 One-Sample Bayes Methods

For non-regular angular distributions, since the corresponding UARS densities are not bounded at $\mathbf{O} = \mathbf{S}$, maximum likelihood methods are not applicable. In such cases one-sample Bayes methods using non-informative priors have been demonstrated to be effective with efficient convergence rates (Bingham, Vardeman and Nordman (3); Bingham, Nordman and Vardeman (4); Qiu, Nordman and Vardeman (11)). Here we briefly review the Bayes methodology and algorithm for posterior simulations.

3.1 Jeffreys Priors

As a prior for the location parameter $\mathbf{S}$, we use the Haar (uniform/invariant) measure on $SO(3)$ with density $p(\mathbf{S}) = 1, \mathbf{S} \in SO(3)$. For the concentration parameter κ, we use a Jeffreys prior. It is slightly more convenient for discussion and plotting purposes to consider the corresponding prior for the spread parameter $\eta = -\log \kappa$ which has a density

$$J(\eta) = \exp(-\eta)\sqrt{\mathcal{I}(\exp(-\eta))} \quad \eta \in (-\infty, \infty)$$

for

$$\mathcal{I}(\kappa) \quad = \quad -E\left(\frac{d^2}{d\kappa^2}\log(C(r|\kappa))\right)$$

In **uarsbayes** the density of the Jeffreys prior for the spread parameter η is calculated using `Jeffreys(eta,model)`.

3.2 MCMC Algorithm

The posterior density $h(\mathbf{S}, \eta)$ for $(\mathbf{S}, \eta)$ is obtained by multiplying the priors with the likelihood function. To generate values from the posterior, we use the Metropolis-Hastings within Gibbs (MHG) algorithm that follows (Bingham, Vardeman and Nordman (3)). With observations $\mathbf{O}_1, ..., \mathbf{O}_n \in SO(3)$ and starting values $\mathbf{S}^0, \eta^0$:

1. As a proposal for $\mathbf{S}^j$, generate $\mathbf{S}^{j^*}$ from the Matrix Fisher rotational distribution with location parameter $\mathbf{S}^{j-1}$ and concentration ρ (Here ρ is a tuning parameter.)
2. Compute $r_j^1 = \frac{h(\mathbf{S}^{j^*}, \eta^{j-1})}{h(\mathbf{S}^{j-1}, \eta^{j-1})}$ and generate $W_j^1 \sim$ Bernoulli$(\min(1, r_j^1))$. Take $\mathbf{S}^j = W_j^1 \mathbf{S}^{j^*} + (1 - W_j^1)\mathbf{S}^{j-1}$.
3. Generate $\eta^{j^*} \sim N(\eta^{j-1}, \sigma^2)$. (Here σ is a tuning parameter.)
4. Compute $r_j^2 = \frac{h(\mathbf{S}^j, \eta^{j^*})}{h(\mathbf{S}^j, \eta^{j-1})}$ and generate $W_j^2 \sim$ Bernoulli$(\min(1, r_j^2))$. Take $\eta^j = W_j^2 \eta^{j^*} + (1 - W_j^2)\eta^{j-1}$.

In **uarsbayes**, the corresponding `R` function is `postsample(data,m,burn,rho,sigma,eta0,S0, model)` where `data` must contain the observed orientations as a $9xn$ matrix, where each row represents one $3x3$ rotation matrix (taken by column). Here `m` is the number of posterior simulations desired, `burn` is the burn-in period desired, `kappa` and `sigma` are the tuning parameters, `eta0` and `S0` are the starting values for the MHG algorithm, and `model` is the chosen member of the UARS class. The values that will be returned by the function are:

- `[[1]]`, m posterior values of η,
- `[[2]]`, m posterior values of $\mathbf{S}$ as a $9 \times m$ matrix, with each column representing an independent 3×3 rotation (taken by column),
- `[[3]]`, the jumping rate of the MHG algorithm for η,
- `[[4]]`, the jumping rate of the MHG algorithm for $\mathbf{S}$.

3.3 Bayes Credible Region

Based on the posterior values for $\mathbf{S}$, a geometrically interpretable credible region for the 3-D location parameter $\mathbf{S}$ can be created. First, define the point estimate $\mathbf{S}_B$ as the maximizer of $tr(\mathbf{S}_B^T\bar{\mathbf{S}})$, where $\bar{\mathbf{S}}$ is the average of the posterior values for $\mathbf{S}$ (Bingham, Vardeman and Nordman (3)). In **uarsbayes** this point estimate is calculated using `bayesShat(S)` where `S` stands for the posterior values of $\mathbf{S}$ generated by `postsample(data,m,burn,rho,sigma,eta0,S0, model)` .

Then an a percent credible region is defined as a set of three cones around the axes of $\mathbf{S}_B$ with angle r, where r is the ath percentile of the maximum arccosine values (between 0 and π) of the diagonal elements of $\mathbf{S}_B^T\mathbf{S}$ where $\mathbf{S}$ stands for the simulated posterior values. In **uarsbayes** the angle of the credible region (in degrees) is calculated using `CL3d(S,level)` and the cone-like credible region for the location parameter can be pictured using `CL3dplot(S,level)` where `S` stands for the posterior values of $\mathbf{S}$ generated by `postsample(data,m,burn,rho,sigma,eta0,S0, model)` and `level` gives the desired level of the credible region.

4 Application to EBSD Data

To illustrate **uarsbayes** and validate its performance, we give an example using data from Bingham, Lograsso and Laabs (1). The data are from an electron backscatter diffraction (EBSD) experiment done to measure crystal orientations in a nickel specimen. Fourteen repeat scans were made on a 2-D rectangular grid on the specimen's planar surface, with over 4000 sites per scan. For this illustration, we use the `ebsd` data set included in the **uarsbayes** package. It consists of a particular 4×28 sub-grid from a single scan on the nickel specimen. It is represented as a 9×112 matrix, where each column consists of the elements from an orientation matrix (by columns) for a specific location.

The goal is to fit both wTN- and vM-UARS models using Bayes methods and to compare the fitted angular distributions to the empirical angular distribution. We simulate 50000 values of the two parameters from the posterior using **uarsbayes** and show that the jumping rates

are as desired.

```
> data(ebsd)
> wtnest<- postsample(data=ebsd,m=100000,
+ burn=50000, rho=2.5,sigma=0.2,eta0=1,
+ S0=diag(1,3,3), model='wTN')
> wtnest[[3]]
[1] 0.341
> wtnest[[4]]
[1] 0.322
> vmest<- postsample(data=ebsd,m=100000,
+ burn=50000, rho=2.2,sigma=2,eta0=1,
+ S0=diag(1,3,3), model='vMises')
> vmest[[3]]
[1] 0.348
> vmest[[4]]
[1] 0.309
```

Here we chose the initial values for the parameters as $\eta^0 = 1, \mathbf{S}^0 = I_{3\times 3}$, but the choices are irrelevant as shown by Bingham, Vardeman and Nordman (3). The tuning parameters are chosen to keep the Metropolis-Hastings jumping rates between 30% and 40%. Then the Bayes estimators for κ and $\mathbf{S}$ can be calculated by using

```
> wtnkappahat<- mean(exp(-wtnest[[1]]))
[1] 0.92
> vmkappahat<- mean(exp(-vmest[[1]]))
[1] 0.27
> wtnShat<- bayesShat(wtnest[[2]])
            [,1]        [,2]       [,3]
[1,]  0.98727735  0.08806978 -0.1323901
```

```
[2,] -0.05429903  0.96928510  0.2398708
[3,]  0.14944913 -0.22963038  0.9617353
> vmShat<- bayesShat(vmest[[2]])
            [,1]        [,2]       [,3]
[1,]  0.99939647 -0.02664991 0.02228191
[2,]  0.02158550  0.97899306 0.20274775
[3,] -0.02721704 -0.20214442 0.97897746
```

The 95% credible region for the location parameter in the wTN-UARS distribution can be displayed as a set of cones (and the angle of these cones can be found) using

```
> CL3d(wtnest[[2]],0.95)
[1] 17.165
> CL3dplot(wtnest[[2]],0.95)
```

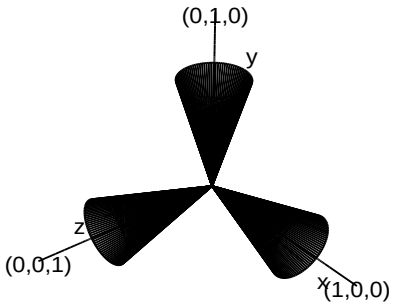

Figure 1 95% Bayes credible region for $\mathbf{S}$ in the wTN model with x, y and z representing the orientation (i.e., column vectors) of the Bayes point estimate.

Using the Bayes estimate of the location parameter $\mathbf{S}$ for both vM and wTN models, we can find the misorientation angles of the `ebsd` observations and plot them against the angles simulated from the corresponding fitted angular distributions in the form of QQplots.

```
qqplot3d(ebsd,wtnShat,wtnkappahat,'wTN')
```

```
qqplot3d(ebsd,vmShat,vmkappahat,'vMises')
```

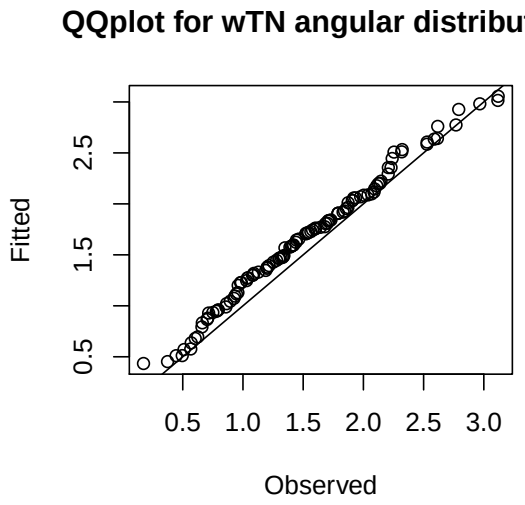

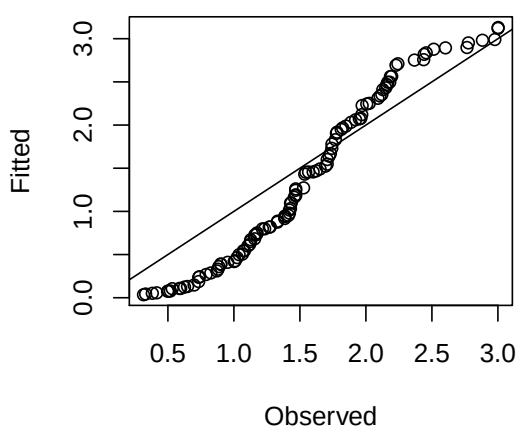

The plots suggest that the fitted wTN-UARS distribution does a better job of describing the nickel specimen across this grid of locations than does the fitted von Mises UARS model.

5 Summary

This package provides practitioners in different fields a tool for analyzing 3-D symmetric orientation data using the UARS class and Bayes inference with non-informative priors. Further development will include quasi-likelihood estimation and Bayes one-way random effects analysis.

Bibliography

[1] M.A. Bingham, B.K. Lograsso and F.C. Laabs A Statistical Analysis of the Variation in Measured Crystal Orientations Obtained Through Electron Backscatter Diffraction. *Journal of Ultramicroscopy* 110:1312-1319,2010.

[2] M.A. Bingham, D.J. Nordman and S.B. Vardeman. Modeling and Inference for Measured Crystal Orientations and a Tractable Class of Symmetric Distributions for Rotations in Three Dimensions. *Journal of the American Statistical Association* 104:1385-1397, 2009a.

[3] M.A. Bingham, S.B. Vardeman and D.J. Nordman. Bayes One-Sample and One-Way Random Effects Analyses for 3-D Orientations with Application to Materials Science. *Bayesian Analysis* 4:607-630, 2009b.

[4] M.A. Bingham, D.J. Nordman and S.B. Vardeman. Finite-Sample Investigation of Likelihood and Bayes Inference for the Symmetric von Mises-Fisher Distribution. *Computational Statistics and Data Analysis* 54:1317-1327, 2009c.

[5] H.J. Bunge. *Texture Analysis in Materials Science*. Butterworth, London, 1982.

[6] T. Chang and L.-P. Rivest. M-Estimation for Location and Regression Parameters in Group Models: A Case Study Using Stiefel Manifolds. *The Annals of Statistics* 29: 784-814, 2001.

[7] C.A. León, J.-C. Massé, and L.-P. Rivest. A Statistical Model for Random Rotations. *Journal of Multivariate Analysis* 97:412-430, 2006.

[8] S. Matthies. Form Effects in the Description of the Orientation Distribution Function (ODF) of Texturized Materials by Model Components. *Physica Status Solidi (b)* 112:705-716, 1982.

[9] S. Matthies, J. Muller, and G.W. Vinel. On the Normal Distribution in the Orientation Space. *Textures and Microstructures* 10:77-96, 1988.

[10] Y. Qiu, D.J. Nordman, and S.B. Vardeman. A Wrapped Trivari- ate Normal Distribution for 3-D Rotations and Bayes Inference. Under review by *Statistic Sinica*, 2012a.

[11] Y. Qiu, D.J. Nordman, and S.B. Vardeman. One-Sample Bayes Inference for Existing Symmetric Distributions on 3-D Rotations. Under review by *Computational Statistics and Data Analysis*, 2012b.

[12] T.I. Savyolova. Preface to *Novye Metody Issledovanija Tekstury Polikristalliĉeskich Materialov*. Metallurgija, Moscow, 1985.

[13] H. Schaeben. The de la Vallée Poussin Standard Orientation Density Function. *Textures and Microstructures* 33:365-373,1997.

CHAPTER 5. SUMMARY

General Conclusion

This paper introduced another distribution in the isotropic UARS family and demonstrate its practice use. Along with that, one-sample Bayes inference has been analyzed for the whole family and demonstrate its effectiveness. All above applications have been programmed into an `R` package for the practitioner's use in the future.

Recommended Future Work

In the real world, there are also many rotations are not isotropic. So possible future research can focus on the transformation of isotropic distributions of rotations to non-isotropic ones.

ACKNOWLEDGEMENTS

I would like to take this opportunity to express my thanks to those who helped me with various aspects of conducting research and the writing of this thesis. First and foremost, Dr. Stephen Vardeman and Dr. Daniel Nordman for their guidance and patience throughout this research and the writing of this thesis. Not only do I have a much better understanding of Statistics, but I also feel like I am better equipped to go into the real world and deal with day to day life.

I would also like to thank my committee members for their efforts and contributions to this work: Dr. Peng Liu, Dr. Max Morris and Dr. Huaiqing Wu.